Extracellular peptide Kratos restricts cell death during vascular development and stress in *Arabidopsis*

Sacha Escamez[1,*,†], Simon Stael[2,3,4,5,†], Julia Vainonen[6,†], Patrick Willems[4,5], Huiting Jin[6], Sachie Kimura[6], Frank Van Breusegem[2,3], Kris Gevaert[4,5], Michael Wrzaczek[6], Hannele Tuominen[1].

[1]Umeå Plant Science Centre, Department of Plant Physiology, Umeå University, Umeå 90187, Sweden

[2] Department of Plant Biotechnology and Bioinformatics, Ghent University, 9052 Ghent, Belgium

[3] VIB-UGent Center for Plant Systems Biology, VIB, 9052 Ghent, Belgium

[4] Department of Biochemistry, Ghent University, 9000 Ghent, Belgium

[5] VIB Center for Medical Biotechnology, 9000 Ghent, Belgium

[6] Organismal and Evolutionary Biology Research Programme, Viikki Plant Science Centre, VIPS, Faculty of Biological and Environmental Sciences, University of Helsinki, Viikinkaari 1 (POB65), FI-00014 Helsinki, Finland

†Shared main authorship.

*Corresponding author:
sacha.escamez@umu.se +46 (0)90 786 8599

Contributing authors' email addresses:

sista@psb.vib-ugent.be; julvai@utu.fi; patrick.willems@ugent.vib.be; huiting.jin@helsinki.fi; sachie.kimura@helsinki.fi; frbre@psb.vib-ugent.be; Kris.Gevaert@UGent.be; michael.wrzaczek@helsinki.fi; hannele.tuominen@umu.se

Highlights

During development or stress response, plants need mechanisms to restrict cell death to the target cells. Kratos is the first plant extracellular peptide found to restrict cell death.

Abstract

During plant vascular development, xylem tracheary elements (TEs) form water-conducting, empty pipes through genetically regulated cell death. Cell death is prevented from spreading to non-TEs by unidentified intercellular mechanisms, downstream of METACASPASE9 (MC9)-mediated regulation of autophagy in TEs. Here, we identified differentially abundant extracellular peptides in vascular-differentiating wild type and *MC9*-downregulated *Arabidopsis* cell suspensions. The peptide Kratos rescued the abnormally high ectopic non-TE death resulting from either *MC9* knockout or TE-specific overexpression of the ATG5 autophagy protein during experimentally induced vascular differentiation in *Arabidopsis* cotyledons. Kratos also reduced cell death following mechanical damage and extracellular ROS production in *Arabidopsis* leaves. Stress-induced but not vascular non-TE cell death was enhanced by another identified peptide, Bia. Bia is therefore reminiscent of several known plant cell death-inducing peptides acting as damage-associated molecular patterns. In contrast, Kratos plays a novel extracellular cell survival role in the context of development and during stress response.

Key words

Arabidopsis, Autophagy, Cell death, Peptide, Peptidomics, Programmed cell death, Stress response, Xylem, Vascular development.

Introduction

Genetically regulated cell death has important roles in stress responses, immunity and development of multicellular organisms (Clarke and Clarke, 1996; Daneva *et al.*, 2016; Galluzzi *et al.*, 2015; Huysmans *et al.*, 2017; Inohara and Nuñez, 2003). Upon stress, infection or developmental stimuli, specific cells become committed to cell death and organized dismantlement. Such cell elimination events, unlike purely accidental cell death, rely on genetic regulation and occur in an anatomically organized manner often referred to as programmed cell death (PCD)(Galluzzi *et al.*, 2015; Lockshin and Williams, 1964; Lockshin and Zakeri, 2001; van Doorn *et al.*, 2011). In contrast to PCD, which implies a mechanism of cell suicide (Reynolds, 2014), cell death can also spread from target cells to neighbouring cells through non-cell autonomous mechanisms (Escamez and Tuominen, 2017; Galluzzi *et al.*, 2015). In animals, a well-known example of such spreading cell death occurs during inflammation (Deretic and Levine, 2018; Kang *et al.*, 2015; Wallach *et al.*, 2014; Zhong *et al.*, 2016). Generally, this latter type of "runaway" cell death, here referred to as "ectopic" cell death, is also genetically regulated even though the underlying molecular mechanisms in plants are poorly understood (Brodersen *et al.*, 2002; Coll *et al.*, 2010; Endo *et al.*, 2001; Escamez *et al.*, 2016; Jabs *et al.*, 1996; Mach *et al.*, 2001; Overmyer *et al.*, 2005; Tuominen *et al.*, 2004; Wrzaczek *et al.*, 2009; Wrzaczek *et al.*, 2015).

While inflammation in animals relies on the same core machinery in different situations (Deretic and Levine, 2018; Kang *et al.*, 2015; Wallach *et al.*, 2014; Zhong *et al.*, 2016), the known instances of plant ectopic cell death seem to involve very different extracellular factors depending on the context (Endo *et al.*, 2001; Escamez *et al.*, 2016; Overmyer *et al.*, 2005; Tuominen *et al.*, 2004; Wrzaczek *et al.*, 2009; Wrzaczek *et al.*, 2015). During the formation of the plant vascular xylem tissue, the water-

conducting tracheary element (TE) cells rid themselves of their protoplasts to form pipe-like structures by undergoing developmental cell death (Escamez and Tuominen, 2014). Dying TEs release molecules that can be harmful to the neighbouring non-TE cells, and restricting subsequent ectopic non-TE cell death requires active regulation (Endo *et al.*, 2001; Escamez *et al.*, 2016). We had previously found that ectopic non-TE cell death increased upon RNAi-based downregulation of the TE-expressed *Arabidopsis* caspase structural homolog METACASPASE9 (MC9) in xylem-differentiating cell suspensions (Escamez *et al.*, 2016).

MC9 downregulation was also associated with an apparent increase in autophagy specifically in the TE cells (Escamez *et al.*, 2016). Autophagy is an evolutionary conserved cellular process that targets cellular components for degradation, either in bulk or in a targeted manner, as a means of posttranslational regulation or for recycling purposes (Bozhkov, 2018; Marshall and Vierstra, 2018). Strikingly, TE-specific downregulation of the autophagy protein ATG2 in the *MC9*-downregulated cells was found to reduce ectopic non-TE death back to wild type levels (Escamez *et al.*, 2016). It therefore seems that ectopic non-TE cell death is regulated by the level of autophagy in TEs, downstream of MC9 (Escamez *et al.*, 2016). The mechanism behind this apparent regulation of autophagy by MC9 remains unknown. None of the core autophagy machinery proteins (Marshall and Vierstra, 2018) appear among the identified targets from MC9-mediated proteolysis, and only a single isoform of one autophagy protein (ATG18b) contains putative MC9 target sites (Tsiatsiani *et al.*, 2013). *Arabidopsis* MC9 and its orthologs in other species have glyceraldehyde-3-phosphate dehydrogenase (GAPDH) as an evolutionary conserved target (Tsiatsiani *et al.*, 2013). GAPDH has been implicated in the regulation of autophagy in several species (Colell *et al.*, 2007; Henry *et al.*, 2015; Tristan *et al.*, 2011), but whether GAPDH could represent the

missing link between MC9 and autophagy, upstream of ectopic cell death, has not been investigated.

Ectopic non-TE death in xylem-differentiating cell suspensions is regulated by MC9 and autophagy in TEs, which implies that ectopic non-TE cell death is regulated in a non-cell-autonomous manner. We therefore sought to identify downstream, extracellular factors that mediate the MC9- and autophagy-dependent regulation of ectopic non-TE death. With MC9 being a protease, and autophagy being involved in secretion of proteins and peptides (e.g. during inflammation in animals)(Kimura *et al.*, 2017a; Kimura *et al.*, 2017b; Zhang *et al.*, 2017), we hypothesized that extracellular peptides could function to regulate ectopic non-TE death downstream of MC9 and autophagy.

Results

Quantitative peptidomics reveals extracellular peptides related to vascular xylem differentiation.

To identify extracellular peptides in the context of vascular xylem differentiation, we used a cell suspension system in which hormonal induction triggers semi-synchronous vascular xylem differentiation over a period of 10 days (Escamez *et al.*, 2016; Pesquet *et al.*, 2010). Triplicate wild type and *MC9*-downregulated (*MC9*-RNAi) cell suspensions were induced to differentiate into xylem TEs and non-TEs, and cells were separated from the extracellular medium by filtration after five days when ectopic cell death starts increasing in *MC9*-RNAi lines (Escamez *et al.*, 2016). Control samples were collected from non-induced wild type and *MC9*-RNAi cell suspensions. Proteins were isolated from the extracellular medium and peptides were separated from the higher molecular weight fraction by filtration over a 3 kDa cut-off filter (Fig. 1a). Immunoblotting of the higher molecular weight fraction (>3kDa) showed no visible

contamination with intracellular proteins (Fig. S1a). The peptide-containing fraction (<3 kDa) was enriched and purified by Solid Phase Extraction (SPE) (Fig. 1a). Subsequently, peptides were identified and quantified by LC-MS/MS using a Q Exactive mass spectrometer resulting in the identification of 1,229 different peptides. Overlapping peptides matching to the same protein sequence, so-called ragged peptides, were assembled into the Longest Peptide Variant (LPV; Fig. 1b)(Secher *et al.*, 2016). After LPV assembly, 722 unique peptides were identified, of which 689 were quantified in at least one replicate of one genotype in one condition (Dataset S1).

The identified peptides showed a bias in amino acid composition, favouring Gly and Pro (Fig. S1b). At the P1 position (position of the precursor protein sequence where cleavage releases the peptide), Gly or Lys were over-represented (Fig. S1b). The fact that MC9 cleaves proteins after Arg or Lys (Tsiatsiani *et al.*, 2013) suggests that a subset of the peptides could result from MC9-mediated cleavage.

Induction of xylem differentiation doubled the peptidome repertoire in both WT and *MC9*-RNAi genotypes (Fig. 1c), likely reflecting an increase in proteolytic processes. Under control conditions the extracellular peptidomes of WT and *MC9*-RNAi largely overlapped (185 peptides, ~80% overlap; Fig. 1c), while they diverged more (254 peptides, ~60% overlap; Fig. 1c) after induction of xylem differentiation. Hence, xylem differentiation increased peptide diversity in a genotype-dependent manner. We reasoned that candidate regulator peptides for ectopic non-TE cell death should fulfil three criteria: (i) such peptides should accumulate during *in vitro* differentiation, (ii) they should be differentially abundant between wild type (low ectopic death) and *MC9*-RNAi cells (elevated ectopic death), and (iii) the corresponding genes should be expressed during vascular differentiation. Based on these criteria, we prioritized a set of 15 candidate peptides for further characterization of their bioactivity (Table S1).

Kratos restricts runaway ectopic cell death during vascular differentiation.

To test the effect of the candidate peptides on ectopic non-TE death, we used the Vascular cell Induction culture System Using Arabidopsis Leaves (VISUAL)(Kondo *et al.*, 2016) system in which differentiation of vascular cells can be induced in the cotyledons (embryonic leaves) of *Arabidopsis thaliana*. This system enables differentiation of TEs within only four days (Kondo *et al.*, 2016), as confirmed by the expression patterns of TE marker genes (Bollhöner *et al.*, 2013; Escamez *et al.*, 2016), and by autofluorescence of lignin in the cell walls of TEs (Fig. S2a-g). VISUAL also allows monitoring non-TE cell death. Unlike TEs that become devoid of any visible content because they undergo complete protoplast autolysis (Escamez and Tuominen, 2017), ectopically dying non-TEs retain their protoplasts which become autofluorescent (Fig. S2h-j). Autofluorescence of non-TE protoplasts was also observed following mechanical wounding of the cotyledons (Fig. S2k-m), suggesting that protoplast autofluorescence could be used as a general hallmark of ectopic cell death in the VISUAL system.

In a first screen, crude synthetic peptide solutions (i.e. without purifying the synthesized peptides) of the 15 candidate peptides were applied to the cotyledons of wild type (Col-0) and MC9 knockout mutant *mc9-2* (Bollhöner *et al.*, 2013) seedlings 24 h after induction of vascular differentiation (Fig. 2a,b; Fig. S3). At this stage the newly transdifferentiated pro-cambial cells start differentiating into other vascular cell types such as TEs (Kondo *et al.*, 2016). In agreement with previous results in *MC9*-RNAi cell suspensions(Escamez *et al.*, 2016), *mc9-2* mutants showed significantly more ectopic non-TE death than wild type seedlings (Fig. 2a,b; Fig S3). Application of three peptides (Peptide 1, Peptides 3 and 4; Table S1), led to a reduction of ectopic non-TE death in *mc9-2* to levels comparable to wild type, without any dose-dependent

effect on TE-differentiation (Fig. 2a; Fig. S3). Peptide 1, but not Peptide 3 or Peptide 4, reduced ectopic non-TE death in a dose-dependent manner (Fig. 2a). An opposite, dose-dependent increase in ectopic non-TE death was observed in both wild type and *mc9-2* genotypes upon treatment with Peptide 14 (Fig. 2b).

In addition to its dose-dependent effect, the candidate Peptide 1 accumulated in the medium of wild type cells, but not upon *MC9* downregulation (Fig. 3a,c; Dataset S1). Peptide 1 is part of a precursor protein of unknown function that contains a repeated motif of GGG(I/V)GGG(I/F)GK as well as six repeats of Peptide 1 (Fig. S4a), suggesting a putative role as a precursor protein for bioactive peptides. The other peptide with a dose-response, the candidate Peptide 14, accumulated only in the medium of differentiating *MC9*-RNAi cells (Fig. 3b,c). The precursor protein of Peptide 14 is part of an uncharacterized protein family founded by the highly conserved small EDRK-rich factor (SERF, previously known as H4F5)(Kelter *et al.*, 2000; Lefebvre *et al.*, 1995; Roy *et al.*, 1995) proteins in metazoans (Fig. S4b,c). We named Peptide 1 (and its corresponding gene/protein AT3G23450) “Kratos”, and Peptide 14 (AT3G24100) “Bia”, in reference to the homonymous children of the Styx river separating the worlds of the living and of the dead in the ancient Greek mythology.

To confirm the cell-survival effect of Kratos, Peptide 3, and Peptide 4, as well as the death-promoting effect of Bia, we repeated the treatments of differentiating cells in the VISUAL system with purified synthetic peptides (purity > 95%). Treatment with purified Kratos confirmed its ability to decrease ectopic non-TE death in *mc9-2* without affecting TE differentiation (Fig. 4a). Furthermore, a knockout T-DNA line for the Kratos-encoding gene (*AT3G23450*; *kratos-1*) - devoid of visible xylem differentiation defect (Fig. S5) - showed a trend towards higher ectopic non-TE death than wild type (Fig. 4a), which could be complemented by treatment with purified Kratos (Fig. 4a). These results,

together with the reduced abundance of extracellular Kratos in differentiating *MC9*-RNAi cell suspensions (Fig. 3c) and the increased ectopic non-TE upon loss of MC9 function (Fig. 2; Fig. 4), indicate that Kratos functions in restricting MC9-dependent ectopic non-TE death during xylem differentiation.

Peptides 3 and 4 were disqualified as potential regulators of ectopic non-TE death based on the inability of the corresponding purified peptides to significantly decrease ectopic non-TE death in *mc9-2* (Fig. S6), and because T-DNA lines for the corresponding genes did not display consistent changes in ectopic death (Fig. S6). The potential role of Bia in promoting ectopic non-TE death during vascular differentiation remained unclear because treatment with the corresponding purified peptides produced inconsistent effects depending on the treated genotype (Fig. 4b). Furthermore, even without treatment ectopic non-TE death tended to increase, rather than decrease, in a T-DNA knockout line for the Bia-encoding gene (*AT3G24100*; *bia-1*; Fig. 4b).

Kratos functions downstream of autophagy in TEs.

Autophagy has been suggested to increase in the TEs of *MC9*-downregulated cell suspensions, which also display elevated ectopic non-TE death (Escamez *et al.*, 2016). Cell-type specific downregulation of the autophagy gene *ATG2* to decrease autophagy in TEs was found sufficient to restrict ectopic non-TE death in *MC9*-downregulated cell suspensions (Escamez *et al.*, 2016). Consistent with the modulation of autophagy by MC9 in TEs, we found a partial co-localization between MC9 and the vascular expressed autophagosome marker ATG8a (Furuta *et al.*, 2014) in TEs in roots of *Arabidopsis* seedlings (Fig. S7a). Visualization of autophagosomes with the same marker showed increased autophagy in the TEs of *mc9-2* compared with the wild type (Fig. S7b). Furthermore, the extracellular medium of xylem differentiating cell suspensions contained six unique peptides matching three subunits of the GAPDH

(Dataset S1) protein, a known regulator of autophagy (Colell *et al.*, 2007; Henry *et al.*, 2015; Tristan *et al.*, 2011), as well as an evolutionary conserved target of MC9 and its orthologs (Tsiatsiani *et al.*, 2013). Five of the six peptides from GAPDH precursor proteins contain potential MC9 cleavage sites (Fig. S8a). Mammalian GAPDH could be cleaved *in vitro* by recombinant *Arabidopsis* MC9 in a dose-dependent manner, while no cleavage was observed in absence of MC9 or in presence of catalytically inactive MC9 (Fig. S8b). Sequence alignment between the assayed mammalian GAPDH and the *Arabidopsis* GAPDH proteins showed a high degree of conservation, including conservation of three potential MC9 cleavage sites (Fig. S8c) between the detected *Arabidopsis* GAPDH-derived peptides (Fig. S8a) and the assayed mammalian protein (Fig. S8c) It is therefore reasonable to hypothesize that MC9 regulates autophagy in TEs by cleaving GAPDH, which would also lead to the release of GAPDH peptides during TE autolysis, thereby explaining that we detected extracellular GAPDH-derived peptides.

Given that TE autophagy modulates ectopic non-TE death downstream of MC9, it is possible that modulation of autophagy in TEs could function upstream of the Kratos-mediated restriction of ectopic non-TE death. To test this hypothesis, we increased the level of autophagy in TEs by overexpressing the autophagy rate-limiting protein ATG5 (Minina *et al.*, 2018) under the transcriptional control of the *IRX1* promoter (pro*IRX1::ATG5*), which is active in TEs and not in non-TEs (Escamez *et al.*, 2016) (Fig. S7c). Overexpression of ATG5 in TEs increased autophagy in these cells (Fig. S7c) without significant effect on TE differentiation compared to wild type (Fig. 4a,b). Instead, consistent with a link between TE autophagy and ectopic non-TE death, ATG5 overexpression in TEs resulted in a significant increase in ectopic non-TE death (Fig. 4a,b). Ectopic non-TE death in pro*IRX1::ATG5* cotyledons was decreased to wild type levels by treatment with Kratos peptide (Fig. 4a). Given that extracellular abundance of Kratos was reduced in cell suspensions where

TEs displayed MC9 downregulation and hence increased autophagy (Fig. 3c), the restriction of ectopic non-TE death in pro*IRX1::ATG5* by Kratos (Fig.4a) suggests that this peptide functions downstream of TE autophagy (Fig. 4c). Unexpectedly, ectopic non-TE death in pro*IRX1::ATG5* was decreased upon treatment with Bia (Fig. 4b), suggesting that the relation between Bia and TE autophagy may be complex.

Kratos and Bia modulate ectopic cell death induced by stress.

The ability of Kratos (Fig. 2a; Fig. 4a) to modulate ectopic cell death during induction of vascular differentiation, and the possible death-promoting effect of Bia (Fig. 2b), prompted us to test whether these peptides could modulate ectopic cell death in other contexts than vascular differentiation.

Mechanical stress was imposed to induce wounding and subsequent ectopic cell death by excision of leaf disks from wild type and *mc9-2* leaves and infiltration with buffer alone or with peptide. Indeed, following local mechanical stress, cell death has been shown to spread from the site of application to other cells (Greenberg and Ausubel, 1993; Wrzaczek *et al.*, 2015). Here, cell death was estimated over time by measuring electrolyte leakage (Fig. 5a). Electrolyte leakage dynamics were comparable between wild type and *mc9-2* (Fig. 5a), as expected from the fact that *MC9* is expressed in cells undergoing developmental, rather than accidental, cell death(Olvera-Carrillo *et al.*, 2015). Cell death increased in both genotypes upon treatment with the Bia peptide (Fig. 5a), consistent with an ectopic cell death-promoting role. Treatment with the Kratos peptide decreased cell death following mechanical stress regardless of the genotype (Fig. 5a), consistent with the ability of Kratos to restrict ectopic cell death.

Additionally, cell death was induced by extracellular reactive oxygen species (ROS) production in leaves of wild type as well as in the null mutants *kratos-1* and *bia-1*, and cell death was measured by

electrolyte leakage after four hours (Fig. 5b). Cell death in response to extracellular ROS production was significantly higher in *kratos-1* plants compared to wild type (Fig. 5b), consistent with an anti-ectopic cell death role for Kratos. The ability of Bia to enhance cell death was also supported by the fact that *bia-1* plants displayed less ectopic cell death than wild type plants (Fig. 5b).

Kratos and Bia regulated cell death in ways which are reminiscent of responses to microbe-associated molecular patters (MAMPs) and/or damage-associated molecular patterns (DAMPs)(Bigeard *et al.*, 2015). MAMPs and DAMPs trigger signalling cascades whose hallmarks include the production of extracellular ROS and activation of mitogen-activated protein kinases (MAPK or MPK), especially MPK3 and MPK6 (Bigeard *et al.*, 2015). We investigated whether Kratos and Bia could modulate ectopic cell death through similar signalling networks. Unlike the MAMP flg22, an epitope of the bacterial flagella which triggers oxidative burst, neither Kratos nor Bia application triggered a ROS burst (Fig. S9). On the other hand, MPK3 and MPK6 activation, which typically peaks within 10-15 min after signal perception (Bigeard *et al.*, 2015), was higher 15 min after infiltration of *Arabidopsis* leaves with Kratos or Bia compared to controls (Fig. S9). Together these results suggest that some downstream responses to Kratos and Bia could be shared with MAMPs or DAMPs while others seem to be distinct.

Our collective results reveal that Kratos has the ability to restrict ectopic cell death both in a normal developmental context and as a consequence of stress, while Bia conclusively promotes ectopic cell death only in the tested stress conditions. At least during xylem differentiation and wounding, cell death can spread in a regulated manner which reveals that the original trigger itself does not necessarily cause all of the observed death events. Instead, the cell death that ectopically spreads likely represents a specific type of cell death with its own genetic regulation (Wrzaczek *et al.*, 2009; Wrzaczek *et al.*, 2015) (Fig. 4a; Fig. 5)

that relies on extracellular peptides (Fig.3-5), one of which apparently functions downstream of autophagy in TEs (Fig. 4a).

Discussion

By combining peptidomics with the use of a controlled plant vascular differentiation system, we identified 1229 extracellular peptides, corresponding to 433 proteins, in the context of plant vascular development (Dataset S1). These numbers, as often with peptidomics, differ from current high mass-accuracy shotgun proteomics. Nevertheless, our analysis performed at least as well as other label-free peptidomics (Chen *et al.*, 2014; Ling *et al.*, 2010; Nanni *et al.*, 2009) studies when considering the caveats associated with endogenous peptidomics (Dallas *et al.*, 2015). One frequently reported challenge in peptidomics is the occurrence of progressively shortened N- or C-terminal peptide ends. Assuming that they belong to the same (bioactive) precursor, we aggregated such ragged peptides to a single longest peptide variant (LPV; Fig. 1b), thereby facilitating data interpretation and enhancing label-free quantitation as the intensity of the LPVs is the sum of the intensities of all their nested peptides. A previous proteomics study identified 149 proteins with an ortholog in *Arabidopsis* in the xylem sap of *Brassica oleracea* (Ligat *et al.*, 2011) but did not focus on the peptide fraction. While the different methods and data processing pipelines between both studies render direct comparison of the detected peptides challenging (Ligat *et al.*, 2011), 27 proteins identified in the xylem sap of *Brassica oleracea* matched precursor proteins of the peptides identified in our dataset (Dataset S1). This suggests that our dataset is relevant for the developmental context of vascular xylem differentiation.

Differentiating TEs undergo developmentally-regulated cell death and protoplast autolysis (Escamez and Tuominen, 2014), during which they release proteases, and likely other molecules, which can either directly

injure and kill neighbouring cells (Endo *et al.*, 2001) or possibly activate signalling towards ectopic cell death (Endo *et al.*, 2001; Escamez *et al.*, 2016). To prevent ectopic non-TE death, it was shown that at least one protease inhibitor must be released in the extracellular medium of xylem-differentiating cell suspensions in *Zinnia elegans* (Endo *et al.*, 2001). We report here the extracellular peptide Kratos as another factor that is required to restrict ectopic non-TE death in *Arabidopsis.* Kratos was abundant in wild type xylem-differentiating cell suspensions (Fig. 3c), and it rescued the ectopic cell death during vascular differentiation in the *mc9-2* mutant (Fig. 2a,4a). Another peptide, Bia, was only detected in the extracellular medium of differentiating, ectopic cell death-prone *MC9*-RNAi cell suspensions (Fig. 3c) and displayed a tendency to promote ectopic cell death following stress (Fig. 5a,b). Our data suggests that ectopic non-TE death is modulated by a balance between pro-death and pro-survival factors. This balance is altered when *MC9* is downregulated (Fig. 3c; Dataset S1), resulting in enhanced ectopic death (Escamez *et al.*, 2016) (Fig. 4,5). We identified the extracellular peptide Kratos as one of these factors regulating runaway ectopic cell death, and possibly also Bia. Neither of the precursor proteins for Bia or Kratos had been found among MC9 targets in *Arabidopsis* seedlings and their cleavage sites do not display the MC9-specific lysine or arginine amino-acid at the P1 position. Hence, Kratos and Bia are likely indirect targets of MC9, possibly through MC9-dependent modulation of TE autophagy (Fig. S7a,b)(Escamez *et al.*, 2016), as seems to be the case for Kratos (Fig. 3c; Fig. 4a).

An important function of MC9 in TEs during vascular development is the regulation of autophagy (Escamez *et al.*, 2016) (Fig. S7b), which in turn regulates non-TE ectopic cell death (Escamez *et al.*, 2016) (Fig. 4a-c). More precisely, our results indicate that MC9 tunes down the level of autophagy in TEs, while TE autophagy negatively regulates the extracellular accumulation of the ectopic cell death-restricting Kratos

peptide (Fig. 4c). Frequent identification of peptides derived from GAPDH (Dataset S1), which is known to regulate autophagy (Colell *et al.*, 2007; Henry *et al.*, 2015; Tristan *et al.*, 2011) and can be cleaved by MC9 (Tsiatsiani *et al.*, 2013)(Fig. S8b), allows to hypothesize that GAPDH cleavage by MC9 could mediate the modulation of autophagy upstream of ectopic cell death.

Autophagy is known as a cellular process in which double-membrane enclosed autophagosome vesicles transport cellular components to vacuoles or lysosomes for degradation and recycling (Marshall and Vierstra, 2018), which seems contradictory with a role in regulating accumulation of extracellular peptides. Yet, studies in animals have found a role for autophagy in secreting proteins or peptides (Bhattacharya *et al.*, 2014; Kimura *et al.*, 2017b), which has also been hypothesized in plants (Pečenková *et al.*, 2017). Hence, TE autophagy may directly regulate extracellular peptide accumulation similar to the secretion of the mammalian pro-inflammatory interleukin-1β (IL-1β) peptide by autophagy (Dupont *et al.*, 2011). TE autophagy may also play a role in degrading an upstream regulator of extracellular peptide accumulation, as observed for mammalian senescence-associated secretory phenotype (SASP)(Kang *et al.*, 2015). A third possibility is that different levels of autophagy in TEs could influence the intracellular content released by TEs upon loss of plasma-membrane integrity during developmental cell death and autolysis.

Intriguingly, while identified in a specific developmental context, both Kratos and Bia possess the ability to modulate ectopic cell death that results from stress. Stress-induced cell death and developmental cell death are known to display distinct transcriptional and anatomical hallmarks (Escamez and Tuominen, 2017; Fendrych *et al.*, 2014; Olvera-Carrillo *et al.*, 2015; Overmyer *et al.*, 2005; Torres *et al.*, 2005; van

Doorn, 2011), indicating that they represent different types of cell death. It is therefore surprising to find that Kratos and Bia can modulate ectopic cell death occurrences that follow different triggers. A possible explanation is that, after stress-induced or developmental cell death, the resulting ectopic cell death represents one specific type of cell death with its own anatomical features and molecular machinery, different from the cell death that is induced directly in response to the initial stimulus. This seems to be the case at least for the ectopic non-TE death which is anatomically distinct from the cell death of the TEs (Escamez *et al.*, 2016) (Fig. S2h-m), and where only the former and not the latter is affected by Kratos (Escamez *et al.*, 2016) (Fig. 2a,4a). The spreading, runaway cell death in plants that follows stress-induced or developmental cell death may therefore be analogous to an inflammation-like response caused by the initial, "primary" cell death. Given our finding that Kratos can restrict runaway ectopic cell death in developmental and stress-related contexts, we hypothesize the existence of a plant inflammation-like response involving Kratos as a canonical effector.

Materials and methods

Plant material and growth conditions.

Cell suspensions from the Col-0 wild type background were previously described (Escamez *et al.*, 2016; Pesquet *et al.*, 2010). The *MC9*-RNAi cell suspensions were generated as previously described (Escamez *et al.*, 2016) by *Agrobacterium*-mediated transformation of wild type cell suspensions. Growth conditions and inductions of vascular xylem-like differentiation were performed as previously described (Escamez *et al.*, 2016).

Arabidopsis genotypes were all in the Col-0 background. The T-DNA knockout line *mc9-2* (SALK_075814) had been previously published (Bollhöner *et al.*, 2013). The T-DNA lines *kratos-1* (SALK_201112) and

bia-1 (SALK_069212) were obtained from the Nottingham Arabidopsis Stock Centre (NASC), and homozygous plants were identified which did not display expression of the corresponding genes (Fig. 10). For identification of knock-out mutants *kratos-1* and *bia-1*, the RNA were isolated with RNeasy plant kit (Qiagen), cDNA synthesis was performed with QuantiTect reverse transcription kit (Qiagen), and semi-quantitative PCRs were run with Go Taq Green Master Mix (Promega) according to manufacturer's instructions (*Bia* forward primer: ATGACTCGAGGAAGTCAAAG; *Bia* reverse primer: TCACTTATTGTTTCCTTTGCCT; *Kratos* forward primer: ATGGGGCGTCTCGTTAGTG; *Kratos* reverse primer: TTAGTGGTGTCCGATTCCG). The transcriptional reporter lines pro*MC9::GUS* and pro*IRX1::GFP:GUS* were previously described (Bollhöner *et al.*, 2013; Escamez *et al.*, 2016). The vascular-expressed autophagasomal fluorescent marker *proATG8a::GFP:ATG8a* and the fluorescently labelled MC9 under the transcriptional control of the *MC9* endogenous promoter pro*MC9::MC9:mCherry* have been previously described (Bollhöner *et al.*, 2013; Furuta *et al.*, 2014).

The overexpressor of the autophagy rate-limiting ATG5 protein (Minina *et al.*, 2018) in TEs pro*IRX1::ATG5* was generated as follows: the *ATG5* full coding sequence was amplified by PCR, using primers including sequences for Gateway BP recombination (forward: GGGGACAAGTTTGTACAAAAAAGCAGCAGGCTTAATGGCG AAGGAAGCGGTCAAG; reverse: GGGGACCACTTTGTACAAGAAAGCTGGGTATCACC TTTGAGGAGCTTTCAC), and recombined using BP clonase into pDONR207 to generate a Gateway-compatible pENTR vector. The *IRX1* promoter fragment (pro*IRX1*; 1586 bp upstream of IRX1/AT4G18780) had previously been inserted instead of the 35S promoter fragment in the Gateway-compatible destination vector pK2GW7 (Escamez *et al.*, 2016; Karimi *et al.*, 2002). This pro*IRX1*-containing destination vector was recombined with the *ATG5*-containing

pENTR vector using LR clonase, resulting in the pro*IRX1::ATG5* binary vector. *Agrobacterium tumefaciens* (stain GV3101) were electroporated with the pro*IRX1::ATG5* binary vector and pro*IRX1::ATG5 Arabidopsis* plants were generated by *Agrobacterium* mediated transformation. pro*IRX1::ATG5* pro*ATG8a::GFP:ATG8a* was generated by crossing.

For induction of vascular differentiation in cotyledons using the VISUAL system, both growth and induction conditions were extensively described previously (Kondo *et al.*, 2016). Each induction of one genotype in one treatment condition included four biological replicates (four seedlings in one and the same well). Plants used for stress-induced cell death assays were grown on soil (peat : vermiculite = 1:1) under white luminescent light (220-250 µmol m^{-2} s^{-1}) at a 12-hour photoperiod (temperature 23/18°C, relative humidity 70/90%) for 5 weeks.

Isolation of extracellular peptides.

Wild type and *MC9*-RNAi cell suspensions were induced to differentiate (or not, as control) in triplicates, each replicate being in a volume of 200 mL (in 1 L Erlenmeyer flasks). After five days, when the rate of TE differentiation is peaking (Escamez *et al.*, 2016), concomitantly with the rise of ectopic non-TE death in MC9-RNAi (Escamez *et al.*, 2016), the samples were harvested. The cells and extracellular medium of each sample were separated using inert sterile membranes with a 0.45 µm pore size (Millipore Stericup-HV Filter Units). The extracellular medium fractions were further filtered using Jumbosep centrifugation devices with a 3 kDa cut-off membrane (Pall) to separate the peptides (< 3 kDa) from higher molecular weight (> 3 kDa) protein (fragments). The higher molecular weight extracellular fraction was compared to cell lysates to verify the absence of detectable intracellular contaminations in the extracellular medium (Fig. S1a). Peptides in the low molecular weight (< 3 kDa) extracellular fraction were further purified by reverse-phase C18 Solid

Phase Extraction (SepPak C18, Waters) and the resulting samples were freeze-dried.

Peptide identification and relative quantification.

Freeze-dried peptide samples were dissolved in 10 µl of 50% acetonitrile (ACN) and subsequently diluted in 200 µl ultrapure water and acidified with trifluoroacetic acid (TFA) to a 1% (v/v) final concentration. No digestion by trypsin or other enzymes was performed, this to preserve the structure of the endogenously generated peptides. 10 µl of each sample were subjected to LC-MS/MS analysis using a Q Exactive mass spectrometer which was operated as previously described (Stes *et al.*, 2014).

Raw mass spectrometry data was searched against TAIR10 representative proteins and contaminant protein sequences by the built-in Andromeda search engine of the MaxQuant software (v1.5.3.30)(Cox and Mann, 2008). The "unspecific cleavage" setting was selected in MaxQuant as no protease was used to prepare the samples. The minimum peptide length was set to eight amino acids, matching-between-runs was enabled with an alignment time of 30 min and matching time window of 30 s. Variable modifications were oxidation of methionine and proline (+15.995 Da), and protein N-terminal acetylation (+42.011 Da). The identified peptides (false discovery rate < 0.01) and their respective intensities were extracted from the "peptides.txt" output file. As trimming of N- and C-terminal ends of peptides was frequently observed, we grouped overlapping peptides to a single longest peptide variant (LPV)(Secher *et al.*, 2016). More specifically, if a peptide sequence was contained within another peptide or extended another peptide by up to three amino acids, both peptides were grouped to a single LPV. The intensity of a LPV is the sum of the intensities of its constituting peptides.

In a next phase, the Perseus (v1.5.4.0) computational platform (Tyanova *et al.*, 2016) was used for quantitative analysis of the

peptidomics data. Peptides matching contaminants, decoy proteins or without an intensity value were omitted, resulting in a list of 689 peptides (Dataset S1). For statistical analyses, only peptides with at least intensity values for two biological replicates in at least one condition were included, resulting in 201 unique peptides compared with statistical tests. Peptide intensities were log10 transformed and missing values were imputed for the total matrix from the normal distribution with a downshift of 1.8 and width of 0.3. Two sample t-tests were performed for pairwise comparisons and the interaction between the condition (induced or not) and genotype effects was tested by a two-way ANOVA test.

The mass spectrometry proteomics data have been deposited to the ProteomeXchange Consortium via the PRIDE(Vizcaíno *et al.*, 2016) partner repository with the dataset identifier PXD010886 (Username: reviewer12401@ebi.ac.uk ; Password: v0LOTVHT).

Preparation of peptide solutions.

Crude, unpurified (35% < purity < 70%, depending on the peptide) peptide synthesis solutions for all the candidate peptides (Table S1) as well as high purity peptide solutions (> 95%) for peptides 3, 4, Kratos and Bia were obtained from GeneCust. All the peptides were dissolved in 10 mM phosphate buffer pH 7 to 1 mM master stocks, taking into account peptide purity in the crude extract to actually obtain 1 mM peptide solutions. Whenever a peptide was visibly insoluble at pH 7, the pH of the master solutions was either lowered with formic acid or increased with ammonia until dissolution was observed. From the 1 mM peptide solutions, master aliquots of 1 µM, 10 µM and 50 µM (1000X solutions) were prepared for experimental use without repeating freezing-thawing cycles.

Microscopy and image analyses.

Samples for promoter-reporter assays with GUS staining were prepared as previously described (Bollhöner *et al.*, 2013). All other cotyledon samples (VISUAL) were fixed and cleared prior to microscopy observation as previously described (Kondo *et al.*, 2016).

All micrographs used for display and quantifications were acquired using an Axioplan II epifluorescence upright microscope equipped with an Axiocam HR color camera. The same imaging settings were conserved for all fluorescence micrographs used for quantifications of TE differentiation and ectopic non-TE death. For instance, images were acquired with a 4x lens, a SOLA SM II LED light source was used for excitation, a dichroic beam splitter allowed blue light excitation (450 nm – 490 nm) and long pass detection of all emission fluorescence from green to red (long pass from 515 nm onward), and an exposure time of 380 ms was used.

Quantifications of cotyledon areas covered with GUS staining, with TEs or with dead non-TEs were performed by manually selecting and measuring the corresponding regions of interest (ROIs) in the open source software Image J. Especially, identification of TE and dead non-TE autofluorescence required manual input from the experimenters due to the fact that the numerous variable features of autofluorescence (cell size, cell shape, layering of cells, autofluorescence intensity, patterned secondary walls…) did not allow for fully automatized segmentation pipelines (Fig. S2n,o). As a result, autofluorescent dead non-TEs were manually identified and selected using the "selection brush tool" in Image J, by several experimenters in parallel and with high number of experiment replication to ensure reproducibility. The selected autofluorescent dead non-TE area was quantified with Image J, as well as the total autofluorescence area of each cotyledon, allowing to deduce the TE autofluorescence area by subtracting the dead non-TE area from the total autofluorescence area.

Confocal laser scanning microscopy analyses were performed as described previously (Escamez *et al.*, 2016), using an inverted Zeiss LSM780 confocal microscope. Imaging for colocalization purposes was performed with a 40x water immersion lens by simultaneous excitation (due to the rapid movement of autophagosomes) of GFP and mCherry with 488 nm and 561 nm lasers (respectively) with a MBS 488/561 beam splitter, and emission detection windows of 495 – 546 nm and 595 – 656 nm, respectively. Colocalization analyses were performed using Image J with the Pearson-Spearman Colocalization (PCS) plugin. For counting of GFP:ATG8a puncta, all compared images within an experiment were acquired with the same settings. To distinguish the puncta from the diffuse GFP fluorescence background, a single threshold for fluorescence intensity in the GFP channel was applied to all the images from a single experiment.

Stress-induced cell death assays.

Mechanical induction of cell death was performed similarly to a previously described study (Wrzaczek *et al.*, 2009). Briefly, fully expanded leaves of five-week-old Col-0 or *mc9-2* plants were infiltrated with 50 nM Kratos, Bia or phosphate buffer as a control. Leaf disks were cut from infiltrated leaves, thereby mechanically inducing cell death. Each leaf disk was placed in 5 mL water, allowing for measurement of ion leakage with a conductivity meter. For MAPK assays, infiltrated leaves were snap frozen in liquid nitrogen 0, 5, 15 and 30 min after infiltration with 50 nM Kratos, Bia or phosphate buffer.

Induction of cell death by oxidative stress using the so-called xanthine/xanthine oxidase (X/XO) system (Jabs *et al.*, 1996) has previously been described (Overmyer *et al.*, 2005). Briefly, fully expanded leaves of five-days-old Col-0, *kratos-1* and *bia-1* plants were detached and infiltrated with a buffer containing superoxide-generating xanthine/xanthine oxidase mixture, or only buffer as a control. After 4h,

the detached leaves were rinsed and cell death from each leaf was quantified by placing the detached leaf in 5 mL water where ion leakage was measured with a conductivity meter, immediately (+0h) or after another 4h (+4h).

Reactive Oxygen Species burst measurements.

Leaf discs were collected using a 4 mm cork borer from 4-week old *Arabidopsis thaliana* Col-0 plants and floated overnight in sterile distilled water in 96 well plate under continuous light at room temperature. On the following day, the water was replaced with assay buffer containing 34 mg/L Luminol sodium salt (Sigma), 20 mg/L horse radish peroxidase (Wako), 100 nM flg22 (GenScript) or synthetic peptides. Luminescence was measured using the GloMax®-Multi+Detection System (Promega). ROS production was expressed in relative luminescence units (RLU). Data are presented as the average of 6 leaves in a representative experiment and the experiment was repeated 3 times with similar results.

Immunoblotting.

Extracellular medium containing proteins >3 kDa after filtration was concentrated using Amicon centrifugal filter units (10 kDa cut-off, Millipore). The control cells were lysed in urea buffer (6M urea, 50 mM Tris-HCl, pH 7.5, protease inhibitor cocktail 1x (Sigma)). Equal protein amount (20-50 µg) separated by SDS-PAGE, transferred to PDVF membranes (BioRad). The membranes were blocked with 5% milk and probed with anti-HSP101 or anti-GDC-H antibody (1:1000 in 1% milk, TBS-T) (Agrisera). Horseradish peroxidase-conjugated donkey anti-rabbit IgG (GE Healthcare) was used as a secondary antibody and the signal was visualized by ECL Prime luminescence reagents (GE Healthcare).

For MAPK kinase assay the frozen leaves were grinded in liquid nitrogen to fine powder and the proteins were extracted by incubation for 30 min at 4°C in extraction buffer (50 mM HEPES, pH 7.4, 50 mM NaCl, 10 mM

EDTA, protease inhibitor cocktail (1x, Sigma), Halt phosphatase inhibitor cocktail (1x, Thermo)) with occasional vortexing. The supernatant after centrifugation at 16000 xg for 10 min at 4°C was used for immunoblotting. 100 µg total protein were separated on 12% SDS-PAGE and transferred to PVDF membrane. The membrane was blocked with 5% milk in TBS and probed with Phospho-p44/42 MAPK antibody (Cell Signaling Technology, #4370; 1:2000 in 1% milk, TBS-T). The signal was detected using fluorescent secondary antibody IRDye800CW Goat anti-Rabbit IgG (LI-COR, # 926-32211) with Odyssey fluorescence scanner (LI-COR Biosciences). Quantification of band intensity was performed with Image J.

GAPDH cleavage analysis

Glyceraldehyde 3-phosphate dehydrogenase (GAPDH) proteins purified from rabbit muscle were purchased from Sigma (#G5262, GAPDH standard for protein electrophoresis and #G2267, GAPDH for enzymatic purposes). Recombinant *Arabidopsis thaliana* MC9 (rMC9) and mutated inactive rMC9$^{C/A}$ (alanine substitution of the active site cysteine) fused to a His-tag were expressed and purified from *E. coli* as previously described (Vercammen *et al.*, 2004). GAPDH proteins were dissolved at 2 mg/ml. A dilution series of rMC9 in Milli-Q purified water was made starting from 1/25 (weight/weight) ratio. A 40 µl reaction mix consisted of 10 µl 4xMC9 buffer (200 mM MES pH 5.5, 600 mM NaCl, 40 % sucrose, 0.4 % CHAPS and 40 mM DTT), 5 µl GAPDH protein and 5 µl of rMC9 or rMC9$^{C/A}$. rMC9 was added to the reaction mix first to auto-activate at room temperature. After 10 minutes, GAPDH protein was added and incubated for 30 minutes at 30 ℃. The reaction was stopped by the addition of 10 µl 5x Laemmli buffer and samples were run on a 4-20 % gradient SDS-PAGE gel (Mini-Protean TGX, Bio-Rad), stained with Instant Blue stain (Expedeon) and imaged with a ChemiDoc Imaging System (Bio-Rad).

Supplementary data

Supplementary figures S1-S10 and table S1, showing more detailed descriptions of the peptidomics results, of the peptides Kratos and Bia, of the experimental procedures followed, and of the experiments validating the materials used, are available online as a spreadsheet file (Table S1) and as a single PDF file (Fig. S1-S10).

Acknowledgements

The authors thank Mikko Luomaranta, Maria Baldauf and Inkeri Soppa for technical assistance. This study was financially supported by PRIME-XS (Grant No. 262067, funded by the European Union 7th Framework Program). S.S. is financially supported by the Flanders Research Foundation (12M3418N). M. W. acknowledges funding from the Academy of Finland (grant numbers #275632, #283139 and #312498) and the University of Helsinki (Three-year fund allocation). H.T. is financially supported by the Swedish Research Council VR (grant number 621-2013-4949) and the Swedish Governmental Agency for Innovation Systems VINNOVA for the UPSC Centre for Forest Biotechnology (grant number 2016-00504).

Author contributions

SE, SS, JV, MW and HT conceived the study and obtained or generated the plant material and peptides. SE generated material from cell suspensions for peptide identification. SS, JV, FVB and KG performed peptide isolation, enrichment, identification, and data interpretation. SE performed all experiments of xylem differentiation. JV, HJ, SK and MW performed stress-induced cell death assays, MPK activity assays, and ROS measurements. SE performed confocal laser scanning microscopy

analyses. SE, SS, MW, KG and HT wrote the manuscript with help from all the other authors.

References

Bhattacharya A, Prakash Y, Eissa NT. 2014. Secretory function of autophagy in innate immune cells. *Cellular microbiology* **16**, 1637-1645.

Bigeard J, Colcombet J, Hirt H. 2015. Signaling mechanisms in pattern-triggered immunity (PTI). *Molecular Plant* **8**, 521-539.

Bollhöner B, Zhang B, Stael S, Denancé N, Overmyer K, Goffner D, Van Breusegem F, Tuominen H. 2013. Post mortem function of AtMC9 in xylem vessel elements. *New Phytologist* **200**, 498-510.

Bozhkov PV. 2018. Plant autophagy: mechanisms and functions. Oxford University Press UK.

Brodersen P, Petersen M, Pike HM, Olszak B, Skov S, Ødum N, Jørgensen LB, Brown RE, Mundy J. 2002. Knockout of Arabidopsis accelerated-cell-death11 encoding a sphingosine transfer protein causes activation of programmed cell death and defense. *Genes & Development* **16**, 490-502.

Chen YL, Lee CY, Cheng KT, Chang WH, Huang RN, Nam HG, Chen YR. 2014. Quantitative peptidomics study reveals that a wound-induced peptide from PR-1 regulates immune signaling in tomato. *Plant Cell* **26**, 4135-4148.

Clarke PG, Clarke S. 1996. Nineteenth century research on naturally occurring cell death and related phenomena. *Anatomy and embryology* **193**, 81-99.

Colell A, Ricci J-E, Tait S, Milasta S, Maurer U, Bouchier-Hayes L, Fitzgerald P, Guio-Carrion A, Waterhouse NJ, Li CW. 2007. GAPDH and autophagy preserve survival after apoptotic cytochrome c release in the absence of caspase activation. *Cell* **129**, 983-997.

Coll NS, Vercammen D, Smidler A, Clover C, Van Breusegem F, Dangl JL, Epple P. 2010. Arabidopsis type I metacaspases control cell death. *Science* **330**, 1393-1397.

Cox J, Mann M. 2008. MaxQuant enables high peptide identification rates, individualized ppb-range mass accuracies and proteome-wide protein quantification. *Nature biotechnology* **26**, 1367.

Dallas DC, Guerrero A, Parker EA, Robinson RC, Gan J, German JB, Barile D, Lebrilla CB. 2015. Current peptidomics: applications, purification, identification, quantification, and functional analysis. *Proteomics* **15**, 1026-1038.

Daneva A, Gao Z, Van Durme M, Nowack MK. 2016. Functions and regulation of programmed cell death in plant development. *Annual Review of Cell and Developmental Biology* **32**, 1-28.

Deretic V, Levine B. 2018. Autophagy balances inflammation in innate immunity. *Autophagy* **14**, 243-251.

Dupont N, Jiang S, Pilli M, Ornatowski W, Bhattacharya D, Deretic V. 2011. Autophagy-based unconventional secretory pathway for extracellular delivery of IL-1β. *The EMBO journal* **30**, 4701-4711.

Endo S, Demura T, Fukuda H. 2001. Inhibition of proteasome activity by the TED4 protein in extracellular space: a novel mechanism for protection of living cells from injury caused by dying cells. *Plant and Cell Physiology* **42**, 9-19.

Escamez S, Tuominen H. 2014. Programmes of cell death and autolysis in tracheary elements: when a suicidal cell arranges its own corpse removal. *Journal of Experimental Botany* **65**, 1313-1321.

Escamez S, André D, Zhang B, Bollhöner B, Pesquet E, Tuominen H. 2016. METACASPASE9 modulates autophagy to confine cell death to the target cells during Arabidopsis vascular xylem differentiation. *Biology Open* **5**, 122-129.

Escamez S, Tuominen H. 2017. Contribution of cellular autolysis to tissular functions during plant development. *Current Opinion in Plant Biology* **35**, 124-130.

Fendrych M, Van Hautegem T, Van Durme M, Olvera-Carrillo Y, Huysmans M, Karimi M, Lippens S, Guérin CJ, Krebs M, Schumacher K. 2014. Programmed cell death controlled by ANAC033/SOMBRERO determines root cap organ size in Arabidopsis. *Current Biology* **24**, 931-940.

Furuta KM, Yadav SR, Lehesranta S, Belevich I, Miyashima S, Heo J-o, Vatén A, Lindgren O, De Rybel B, Van Isterdael G. 2014. Arabidopsis NAC45/86 direct sieve element morphogenesis culminating in enucleation. *Science* **345**, 933-937.

Galluzzi L, Bravo-San Pedro J, Vitale I, Aaronson S, Abrams J, Adam D, Alnemri E, Altucci L, Andrews D, Annicchiarico-Petruzzelli M. 2015. Essential versus accessory aspects of cell death: recommendations of the NCCD 2015. *Cell Death & Differentiation* **22**, 58-73.

Greenberg JT, Ausubel FM. 1993. Arabidopsis mutants compromised for the control of cellular damage during pathogenesis and aging. *The Plant Journal* **4**, 327-341.

Henry E, Fung N, Liu J, Drakakaki G, Coaker G. 2015. Beyond glycolysis: GAPDHs are multi-functional enzymes involved in regulation of ROS, autophagy, and plant immune responses. *Plos Genetics* **11**, e1005199.

Huysmans M, Lema S, Coll NS, Nowack MK. 2017. Dying two deaths—programmed cell death regulation in development and disease. *Current Opinion in Plant Biology* **35**, 37-44.

Inohara N, Nuñez G. 2003. Cell death and immunity: NODs: intracellular proteins involved in inflammation and apoptosis. *Nature Reviews Immunology* **3**, 371.

Jabs T, Dietrich RA, Dangl JL. 1996. Initiation of runaway cell death in an Arabidopsis mutant by extracellular superoxide. *Science* **273**, 1853-1856.

Kang C, Xu Q, Martin TD, Li MZ, Demaria M, Aron L, Lu T, Yankner BA, Campisi J, Elledge SJ. 2015. The DNA damage response induces inflammation and senescence by inhibiting autophagy of GATA4. *Science* **349**, aaa5612.

Karimi M, Inzé D, Depicker A. 2002. GATEWAY™ vectors for Agrobacterium-mediated plant transformation. *Trends in Plant Science* **7**, 193-195.

Kelter A-R, Herchenbach J, Wirth B. 2000. The transcription factor-like nuclear regulator (TFNR) contains a novel 55-amino-acid motif repeated nine times and maps closely to SMN1. *Genomics* **70**, 315-326.

Kimura T, Jia J, Claude-Taupin A, Kumar S, Choi SW, Gu Y, Mudd M, Dupont N, Jiang S, Peters R. 2017a. Cellular and molecular mechanism for secretory autophagy. *Autophagy* **13**, 1084-1085.

Kimura T, Jia J, Kumar S, Choi SW, Gu Y, Mudd M, Dupont N, Jiang S, Peters R, Farzam F. 2017b. Dedicated SNAREs and specialized TRIM cargo receptors mediate secretory autophagy. *The EMBO journal* **36**, 42-60.

Kondo Y, Nurani AM, Saito C, Ichihashi Y, Saito M, Yamazaki K, Mitsuda N, Ohme-Takagi M, Fukuda H. 2016. Vascular Cell Induction Culture System Using Arabidopsis Leaves (VISUAL)

Reveals the Sequential Differentiation of Sieve Element-like Cells. *The Plant Cell*, tpc. 00027.02016.

Lefebvre S, Bürglen L, Reboullet S, Clermont O, Burlet P, Viollet L, Benichou B, Cruaud C, Millasseau P, Zeviani M. 1995. Identification and characterization of a spinal muscular atrophy-determining gene. *Cell* **80**, 155-165.

Ligat L, Lauber E, Albenne C, Clemente HS, Valot B, Zivy M, Pont-Lezica R, Arlat M, Jamet E. 2011. Analysis of the xylem sap proteome of Brassica oleracea reveals a high content in secreted proteins. *Proteomics* **11**, 1798-1813.

Ling XB, Lau K, Deshpande C, Park JL, Milojevic D, Macaubas C, Xiao C, Lopez-Avila V, Kanegaye J, Burns JC, Cohen H, Schilling J, Mellins ED. 2010. Urine Peptidomic and Targeted Plasma Protein Analyses in the Diagnosis and Monitoring of Systemic Juvenile Idiopathic Arthritis. *Clin Proteomics* **6**, 175-193.

Lockshin RA, Williams CM. 1964. Programmed cell death—II. Endocrine potentiation of the breakdown of the intersegmental muscles of silkmoths. *Journal of Insect Physiology* **10**, 643-649.

Lockshin RA, Zakeri Z. 2001. Programmed cell death and apoptosis: origins of the theory. *Nat Rev Mol Cell Biol* **2**, 545-550.

Mach JM, Castillo AR, Hoogstraten R, Greenberg JT. 2001. The Arabidopsis-accelerated cell death gene ACD2 encodes red chlorophyll catabolite reductase and suppresses the spread of disease symptoms. *Proceedings of the National Academy of Sciences* **98**, 771-776.

Marshall RS, Vierstra RD. 2018. Autophagy: The Master of Bulk and Selective Recycling. *Annual Review of Plant Biology*.

Minina EA, Moschou PN, Vetukuri RR, Sanchez-Vera V, Cardoso C, Liu Q, Elander PH, Dalman K, Beganovic M, Yilmaz JL. 2018. Transcriptional stimulation of rate-limiting components of the autophagic pathway improves plant fitness. *Journal of Experimental Botany*.

Nanni P, Levander F, Roda G, Caponi A, James P, Roda A. 2009. A label-free nano-liquid chromatography-mass spectrometry approach for quantitative serum peptidomics in Crohn's disease patients. *J Chromatogr B Analyt Technol Biomed Life Sci* **877**, 3127-3136.

Olvera-Carrillo Y, Van Bel M, Van Hautegem T, Fendrych M, Huysmans M, Simaskova M, Van Durme M, Buscaill P, Rivas S, Coll NS. 2015. A conserved core of programmed cell death

indicator genes discriminates developmentally and environmentally induced programmed cell death in plants. *Plant Physiology* **169**, 2684-2699.

Overmyer K, Brosché M, Pellinen R, Kuittinen T, Tuominen H, Ahlfors R, Keinänen M, Saarma M, Scheel D, Kangasjärvi J. 2005. Ozone-induced programmed cell death in the Arabidopsis radical-induced cell death1 mutant. *Plant Physiology* **137**, 1092-1104.

Pečenková T, Marković V, Sabol P, Kulich I, Žárský V. 2017. Exocyst and autophagy-related membrane trafficking in plants. *Journal of Experimental Botany* **69**, 47-57.

Pesquet E, Korolev AV, Calder G, Lloyd CW. 2010. The Microtubule-Associated Protein AtMAP70-5 regulates secondary wall patterning in Arabidopsis wood cells. *Current Biology* **20**, 744-749.

Reynolds AS. 2014. The deaths of a cell: how language and metaphor influence the science of cell death. *Studies in History and Philosophy of Science Part C: Studies in History and Philosophy of Biological and Biomedical Sciences* **48**, 175-184.

Roy N, Mahadevan MS, McLean M, Shutter G, Yaraghi Z, Farahani R, Baird S, Besner-Johnston A, Lefebvre C, Kang X. 1995. The gene for neuronal apoptosis inhibitory protein is partially deleted in individuals with spinal muscular atrophy. *Cell* **80**, 167-178.

Secher A, Kelstrup CD, Conde-Frieboes KW, Pyke C, Raun K, Wulff BS, Olsen JV. 2016. Analytic framework for peptidomics applied to large-scale neuropeptide identification. *Nature communications* **7**, 11436.

Stes E, Laga M, Walton A, Samyn N, Timmerman E, De Smet I, Goormachtig S, Gevaert K. 2014. A COFRADIC protocol to study protein ubiquitination. *Journal of proteome research* **13**, 3107-3113.

Torres MA, Jones JD, Dangl JL. 2005. Pathogen-induced, NADPH oxidase–derived reactive oxygen intermediates suppress spread of cell death in Arabidopsis thaliana. *Nature Genetics* **37**, 1130.

Tristan C, Shahani N, Sedlak TW, Sawa A. 2011. The diverse functions of GAPDH: views from different subcellular compartments. *Cellular signalling* **23**, 317-323.

Tsiatsiani L, Timmerman E, De Bock P-J, Vercammen D, Stael S, Van De Cotte B, Staes A, Goethals M, Beunens T, Van Damme P. 2013. The Arabidopsis metacaspase9 degradome. *The Plant Cell Online* **25**, 2831-2847.

Tuominen H, Overmyer K, KeinaÈnen M, Kollist H, Kangasjärvi J. 2004. Mutual antagonism of ethylene and jasmonic acid regulates ozone-induced spreading cell death in Arabidopsis. *The Plant Journal* **39**, 59-69.

Tyanova S, Temu T, Sinitcyn P, Carlson A, Hein MY, Geiger T, Mann M, Cox J. 2016. The Perseus computational platform for comprehensive analysis of (prote) omics data. *Nature methods* **13**, 731.

Wallach D, Kang T-B, Kovalenko A. 2014. Concepts of tissue injury and cell death in inflammation: a historical perspective. *Nature Reviews Immunology* **14**, 51.

van Doorn WG. 2011. Classes of programmed cell death in plants, compared to those in animals. *Journal of Experimental Botany* **62**, 4749-4761.

van Doorn WG, Beers EP, Dangl JL, Franklin-Tong VE, Gallois P, Hara-Nishimura I, Jones AM, Kawai-Yamada M, Lam E, Mundy J, Mur LAJ, Petersen M, Smertenko A, Taliansky M, Van Breusegem F, Wolpert T, Woltering E, Zhivotovsky B, Bozhkov PV. 2011. Morphological classification of plant cell deaths. *Cell Death & Differentiation* **18**, 1241-1246.

Vercammen D, van de Cotte B, De Jaeger G, Eeckhout D, Casteels P, Vandepoele K, Vandenberghe I, Van Beeumen J, Inze D, Van Breusegem F. 2004 Type II metacaspases Atmc4 and Atmc9 of Arabidopsis thaliana cleave substrates after arginine and lysine. *Journal of biological chemistry* **279**, 45329-45336.

Vizcaíno JA, Csordas A, Del-Toro N, Dianes JA, Griss J, Lavidas I, Mayer G, Perez-Riverol Y, Reisinger F, Ternent T. 2016. 2016 update of the PRIDE database and its related tools. *Nucleic acids research* **44**, D447-D456.

Wrzaczek M, Brosche M, Kollist H, Kangasjarvi J. 2009. Arabidopsis GRI is involved in the regulation of cell death induced by extracellular ROS. *Proc Natl Acad Sci USA* **106**, 5412 - 5417.

Wrzaczek M, Vainonen JP, Stael S, Tsiatsiani L, Gauthier A, Kaufholdt D, Bollhöner B, Lamminmäki A, Staes A, Gevaert K. 2015. GRIM REAPER peptide binds to receptor kinase PRK5 to trigger cell death in Arabidopsis. *The EMBO journal* **34**, 55-66.

Zhang T, Vavylonis D, Durachko DM, Cosgrove DJ. 2017. Nanoscale movements of cellulose microfibrils in primary cell walls. *Nature Plants* **3**, 17056.

Zhong Z, Sanchez-Lopez E, Karin M. 2016. Autophagy, inflammation, and immunity: a troika governing cancer and its treatment. *Cell* **166**, 288-298.

Figure legends

Figure 1: Peptidomics approach to identify METACASPASE9-regulated extracellular peptides.

(A) Schematic representation of the bioactive peptide identification workflow. The extracellular media of differentiating cell suspensions were sampled five days after induction (n = 3 biological replicates), half-way through the differentiation when *MC9* expression peaks and when ectopic cell death starts increasing in *MC9*-RNAi lines (ref. 16).

(B) Visual explanation for the longest peptide variant (LPV) approach.

(C) Venn diagram showing the number of unique peptides per genotype and per condition (induced or non-induced control).

Figure 2: Unpurified peptides Kratos and Bia affect non-TE death in a dose-dependent manner.

(A) TE differentiation (left) and non-TE death (right) 96h after induction with the VISUAL method of Col-0 wild type and *mc9-2* METACASPASE9 knockout mutant treated with increasing concentrations of Kratos/Peptide 1 (or only phosphate buffer as a control). Error bars represent standard deviation (n = 3 biological replicates). Data points that do not share any letter are significantly different according to post-ANOVA Fischer test ($p < 0.05$).

(B) TE differentiation (left) and non-TE death (right) 96h after induction with the VISUAL method of Col-0 wild type and *mc9-2* METACASPASE9 knockout mutant treated with increasing concentrations of Bia/Peptide 14 (or only phosphate buffer as a control). Error bars represent standard deviation (n = 3 biological replicates). Data points that do not share any letter are significantly different according to post-ANOVA Fischer test ($p < 0.05$).

Figure 3: METACASPASE9-dependent accumulation of the peptides Kratos and Bia.

(A) The assembly of the Longest Peptide Variant (LPV) from the extracellular peptides matching the glycine rich peptide Kratos/Peptide1 derived from the unknown protein AT3G23450 (Table S1).

(B) The assembly of the Longest Peptide Variant (LPV) from the extracellular peptides matching the Small EDRK-Rich Factor (SERF) peptide Bia/Peptide 14 derived from the uncharacterized protein AT3G24100 (Table S1).

(C) Illustration of mass spectrometry identification of the longest identified peptide in (a) and charts displaying quantifications of the average LFQ (label free quantification) intensity for the LPV Kratos/Peptide 1 and Bia/Peptide 14 in the different genotypes and conditions. Error bars represent standard error of the mean (n = 3 biological replicates).

Figure 4: Ectopic non-TE death is restricted by the Kratos peptide during induced vascular differentiation in cotyledons.

(A) TE differentiation (left) and non-TE death (right) 96h after induction with the VISUAL method of Col-0, *mc9-2*, *kratos-1* knockout mutant and pro*IRX1::ATG5* TE autophagy inducer line with or without 50nM Kratos. Error bars represent standard deviation (n = 9 replicate experiments for Col-0 and *mc9-2*, 5 for Col-0 + Kratos, *mc9-2* + Kratos, *kratos-1* and *kratos-1* + Kratos, 4 for pro*IRX1::ATG5* and 3 for pro*IRX1::ATG5* + Kratos, each with 3 biological replicates). Data points that do not share any letter are significantly different according to post-ANOVA Fischer test ($p < 0.05$).

(B) TE differentiation (left) and non-TE death (right) 96h after induction with the VISUAL method of Col-0, mc9-2, *bia-1* knockout mutant and pro*IRX1::ATG5* TE autophagy inducer line with or without 50nM Bia. Error bars represent standard deviation (n = 9 for Col-0 and *mc9-2*, 8 for Col-0 + Bia and *mc9-2* + Bia, 4 for pro*IRX1::ATG5* and 3 for *bia-1*, *bia-1* + Bia and pro*IRX1::ATG5* + Bia, each with 3 biological replicates). Data points that do not share any letter are significantly different according to post-ANOVA Fischer test ($p < 0.05$).

(C) Hypothetical model for the modulation of non-TE ectopic death by MC9 and autophagy in TEs through regulation of extracellular accumulation of the Kratos peptide.

Figure 5: Peptides Kratos and Bia have the ability to modulate stress-induced cell death

(A) Mechanically induced cell death (measured by ion leakage) in leaf disks from Col-0 wild type or *mc9-2* leaves infiltrated with Kratos or Bia peptides, or with buffer as a control. Data points indicate average values while error bars represent standard deviation (n = 4 biological

replicates). Asterisks indicate significantly different ($p < 0.05$) ion leakage dynamics compared with buffer control.

(B) Cell death induced by **4h** treatment with superoxide-generating xanthine/xanthine oxidase (X/XO) and quantified by measuring ion leakage in detached leaves from Col-0, *kratos-1* and *bia-1* 0h (+0h) or 4h (+4h) after the end of the 4h treatment. Bars indicate average values while error bars represent standard deviation (n = 4 biological replicates). Data points that do not share any letter are significantly different according to post-ANOVA Fischer test ($p < 0.05$). The experiments have been repeated twice with similar results.

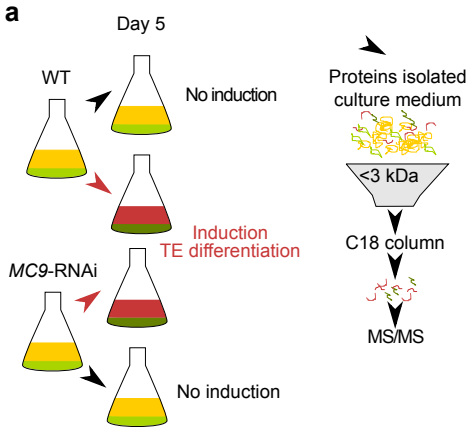

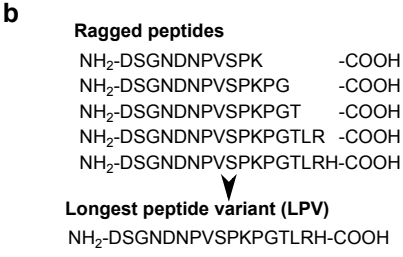

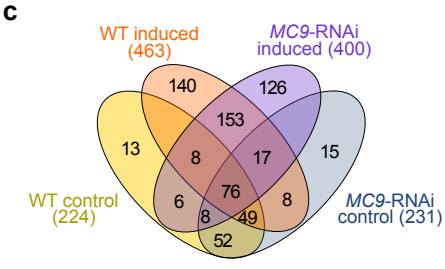

Figure 1: Peptidomics approach to identify METACASPASE9-regulated extracellular peptides.
(a) Schematic representation of the bioactive peptide identif cation workf ow. The extracellular media of dif erentiating cell suspensions were sampled f ve days after induction (n = 3 biological replicates), half-way through the dif erentiation when *MC9* expression peaks and when ectopic cell death starts increasing in *MC9*-RNAi lines (ref. 16).
(b) Visual explanation for the longest peptide variant (LPV) approach.
(c) Venn diagram showing the number of unique peptides per genotype and per condition (induced or non-induced control).

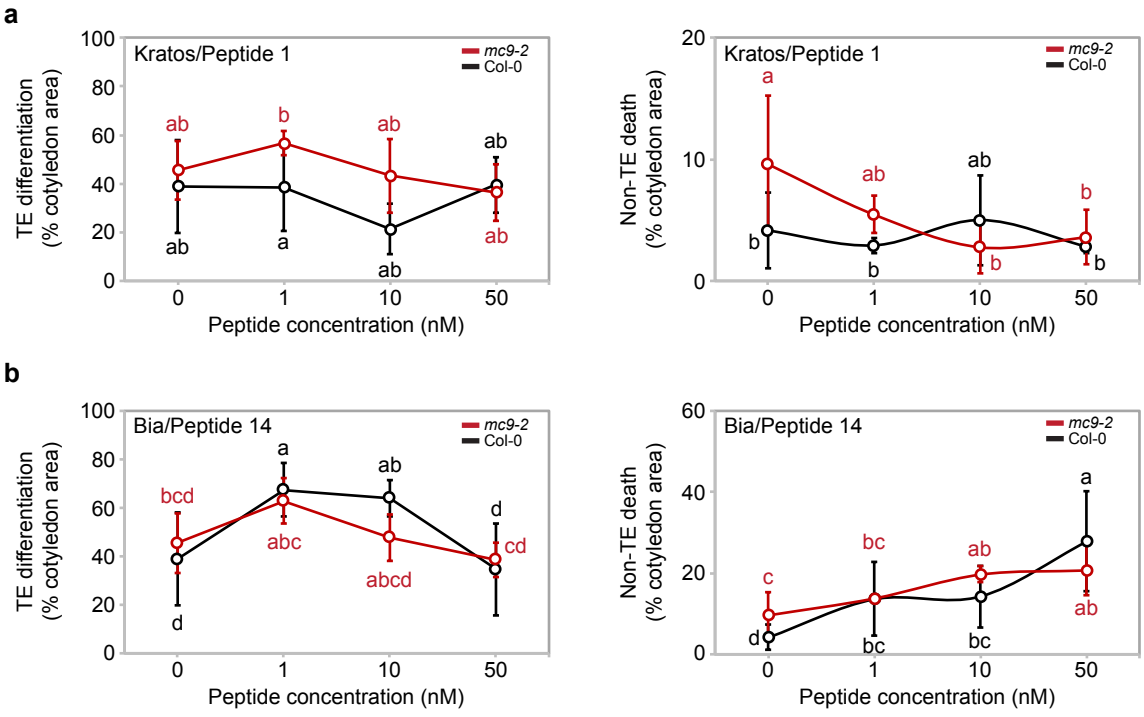

Figure 2: Figure 2: Unpurif ed peptides Kratos and Bia af ect non-TE death in a dose-dependent manner.
(a) TE dif erentiation (left) and non-TE death (right) 96h after induction with the VISUAL method of Col-0 wild type and *mc9-2* METACASPASE9 knockout mutant treated with increasing concentrations of Kratos/Peptide 1 (or only phosphate buf er as a control). Error bars represent standard deviation (n = 3 biological replicates). Data points that do not share any letter are signif cantly dif erent according to post-ANOVA Fischer test ($p < 0.05$).
(b) TE dif erentiation (left) and non-TE death (right) 96h after induction with the VISUAL method of Col-0 wild type and *mc9-2* METACASPASE9 knockout mutant treated with increasing concentrations of Bia/Peptide 14 (or only phosphate buf er as a control). Error bars represent standard deviation (n = 3 biological replicates). Data points that do not share any letter are signif cantly dif erent according to post-ANOVA Fischer test ($p < 0.05$).

a

142 - GGIGKGGGIGGGIG - 155
166 - KGGGIGGGIGKGGGIG - 181
162 - GGIGKGGGIGGGIGKGGGIG - 181

LPV

NH_2-GGIGKGGGIGGGIGKGGGIG-COOH

b

46- TAKKAAQAAAAASSGGGGGKGNNK-69
44-EKTAKKAAQAAAAASSGGGGGKGNNK-69

LPV

NH_2-EKTAKKAAQAAAAASSGGGGGKGNNK-COOH

c

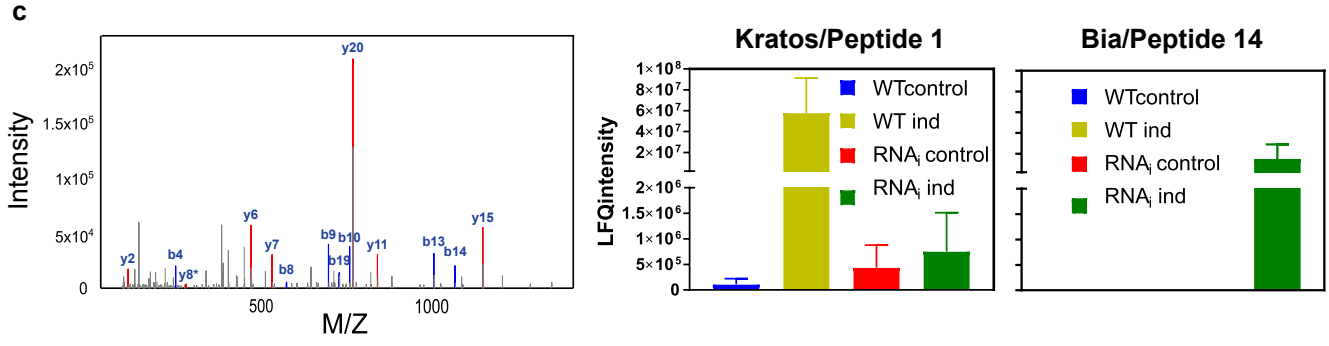

Figure 3: METACASPASE9-dependent accumulation of the peptides Kratos and Bia.
(a) The assembly of the Longest Peptide Variant (LPV) from the extracellular peptides matching the glycine rich peptide Kratos/Peptide1 derived from the unknown protein AT3G23450 (Table S1).
(b) The assembly of the Longest Peptide Variant (LPV) from the extracellular peptides matching the Small EDRK-Rich Factor (SERF) peptide Bia/Peptide 14 derived from the uncharacterized protein AT3G24100 (Table S1).
(c) Illustration of mass spectrometry identif cation of the longest identif ed peptide in (a) and charts displaying quantif - cations of the average LFQ (label free quantif cation) intensity for the LPV Kratos/Peptide 1 and Bia/Peptide 14 in the dif erent genotypes and conditions. Error bars represent standard error of the mean (n = 3 biological replicates).

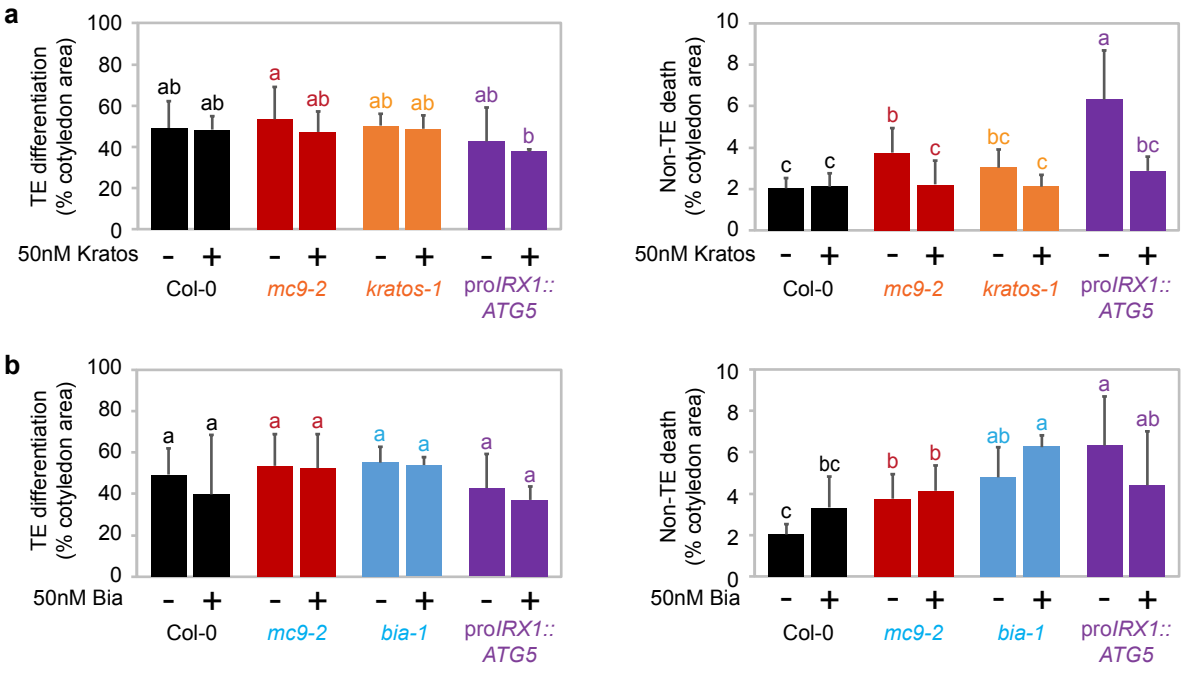

Figure 4: Ectopic non-TE death is restricted by the Kratos peptide during induced vascular dif erentiation in cotyledons.

(a) TE dif erentiation (left) and non-TE death (right) 96h after induction with the VISUAL method of Col-0, *mc9-2*, *kratos-1* knockout mutant and pro*IRX1::ATG5* TE autophagy inducer line with or without 50nM Kratos. Error bars represent standard deviation (n = 9 replicate experiments for Col-0 and *mc9-2*, 5 for Col-0 + Kratos, *mc9-2* + Kratos, *kratos-1* and *kratos-1* + Kratos, 4 for pro*IRX1::ATG5* and 3 for pro*IRX1::ATG5* + Kratos, each with 3 biological replicates). Data points that do not share any letter are signif cantly dif erent according to post-ANOVA Fischer test ($p < 0.05$).

(b) TE dif erentiation (left) and non-TE death (right) 96h after induction with the VISUAL method of Col-0, *mc9-2*, *bia-1* knockout mutant and pro*IRX1::ATG5* TE autophagy inducer line with or without 50nM Bia. Error bars represent standard deviation (n = 9 for Col-0 and *mc9-2*, 8 for Col-0 + Bia and *mc9-2* + Bia, 4 for pro*IRX1::ATG5* and 3 for *bia-1*, *bia-1* + Bia and pro*IRX1::ATG5* + Bia, each with 3 biological replicates). Data points that do not share any letter are signif cantly dif erent according to post-ANOVA Fischer test ($p < 0.05$).

(c) Hypothetical model for the modulation of non-TE ectopic death by MC9 and autophagy in TEs through regulation of extracellular accumulation of the Kratos peptide.

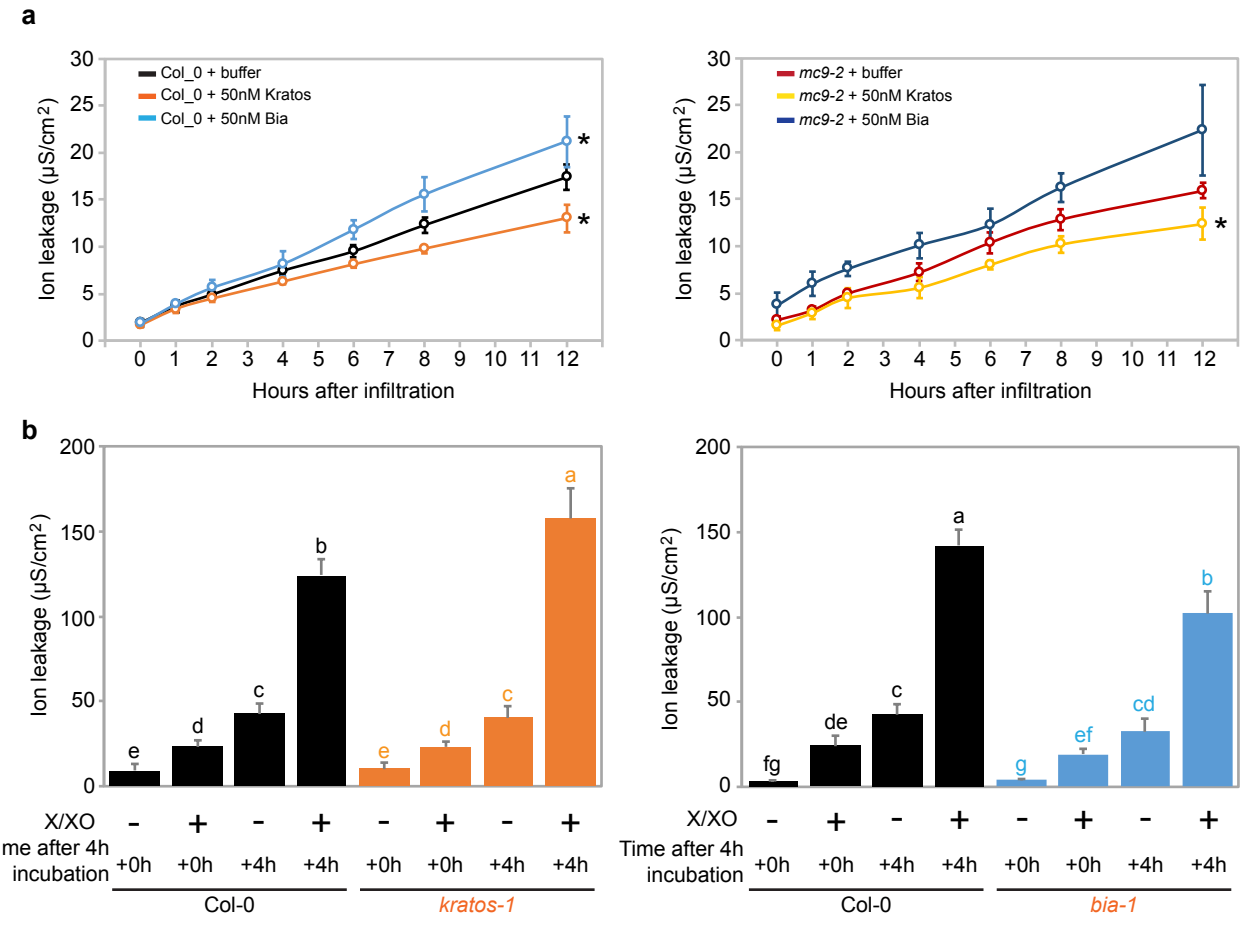

Figure 5: Peptides Kratos and Bia have the ability to modulate stress-induced cell death

(a) Mechanically induced cell death (measured by ion leakage) in leaf disks from Col-0 wild type or *mc9-2* leaves inf ltrated with Kratos or Bia peptides, or with buf er as a control. Data points indicate average values while error bars represent standard deviation (n = 4 biological replicates). Asterisks indicate signif cantly dif erent ($p < 0.05$) ion leakage dynamics compared with buf er control.

(b) Cell death induced by 4h treatment with superoxide-generating xanthine/xanthine oxidase (X/XO) and quantif ed by measuring ion leakage in detached leaves from Col-0, *kratos-1* and *bia-1* 0h (+0h) or 4h (+4h) after the end of the 4h treatment. Bars indicate average values while error bars represent standard deviation (n = 4 biological replicates). Data points that do not share any letter are signif cantly dif erent according to post-ANOVA Fischer test ($p < 0.05$). The experiments have been repeated twice with similar results.

Figure S1: Identification of knockout T-DNA lines for Kratos and Bia
Semi-quantitative PCR comparing transcript levels (full length coding sequence: CDS) of Kratos and Bia between T-DNA lines for these genes (*kratos-1* and *bia-1*, respectively) and wild-type (and *mc9-2* for Kratos). At least three plants of each genotype have been pooled before RNA isolation.

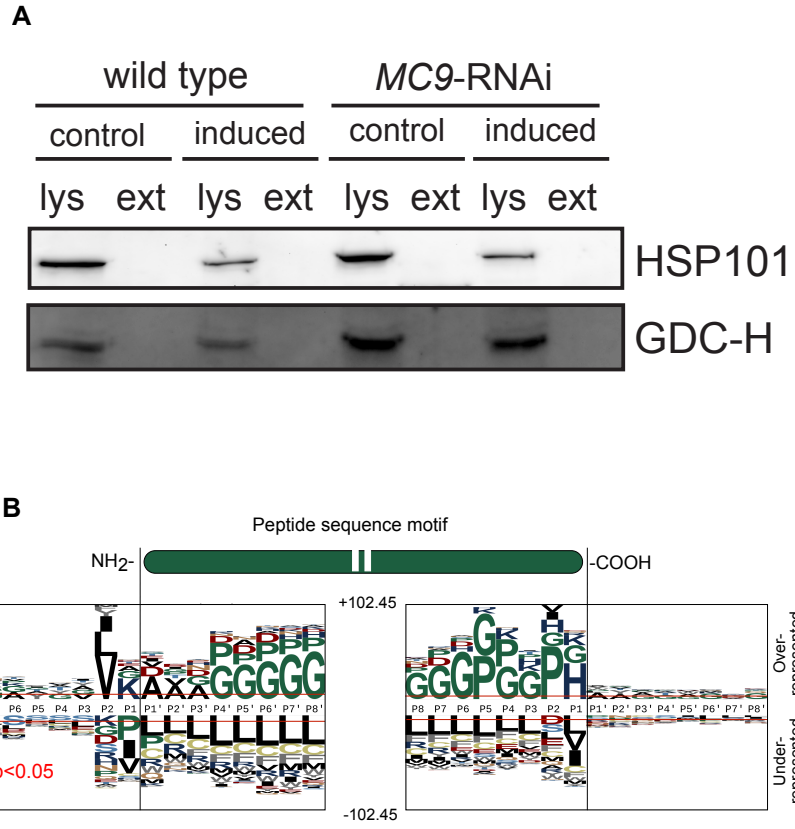

Figure S2: Quantitative peptidomics on extracellular medium of xylogenic *Arabidopsis* cell suspensions.
(A) Western blot analysis of cell lysate (lys) amd extracellular medium (ext) fractions after separation by filtration, to control for possible contamination of the extracellular fraction by intracellular proteins. HSP101 is a cytosolic heat shock protein (101kDa). GDC-H is a mitochondrial glycine decarboxylase complex subunit.
(B) Peptide sequence motif for all 1229 identified peptides generated by pLogo, which visualizes the probability of occurrence of a certain amino acid in a certain position relative to the amino acid distribution of the *Arabidopsis* proteome. The left box visualizes the 8 amino acids surrounding the N-terminal end of the endogenous peptides (labeled P8 till P1 and P1'till P8'), while the right box visualizes those surrounding the C-terminus. This analysis was performed using pLogo (O'Shea JP, Chou MF, Quader SA, Ryan JK, Church GM, & Schwartz D. 2013. pLogo: A probabilistic approach to visualizing sequence motifs. Nat Methods 10, 1211-1212.).

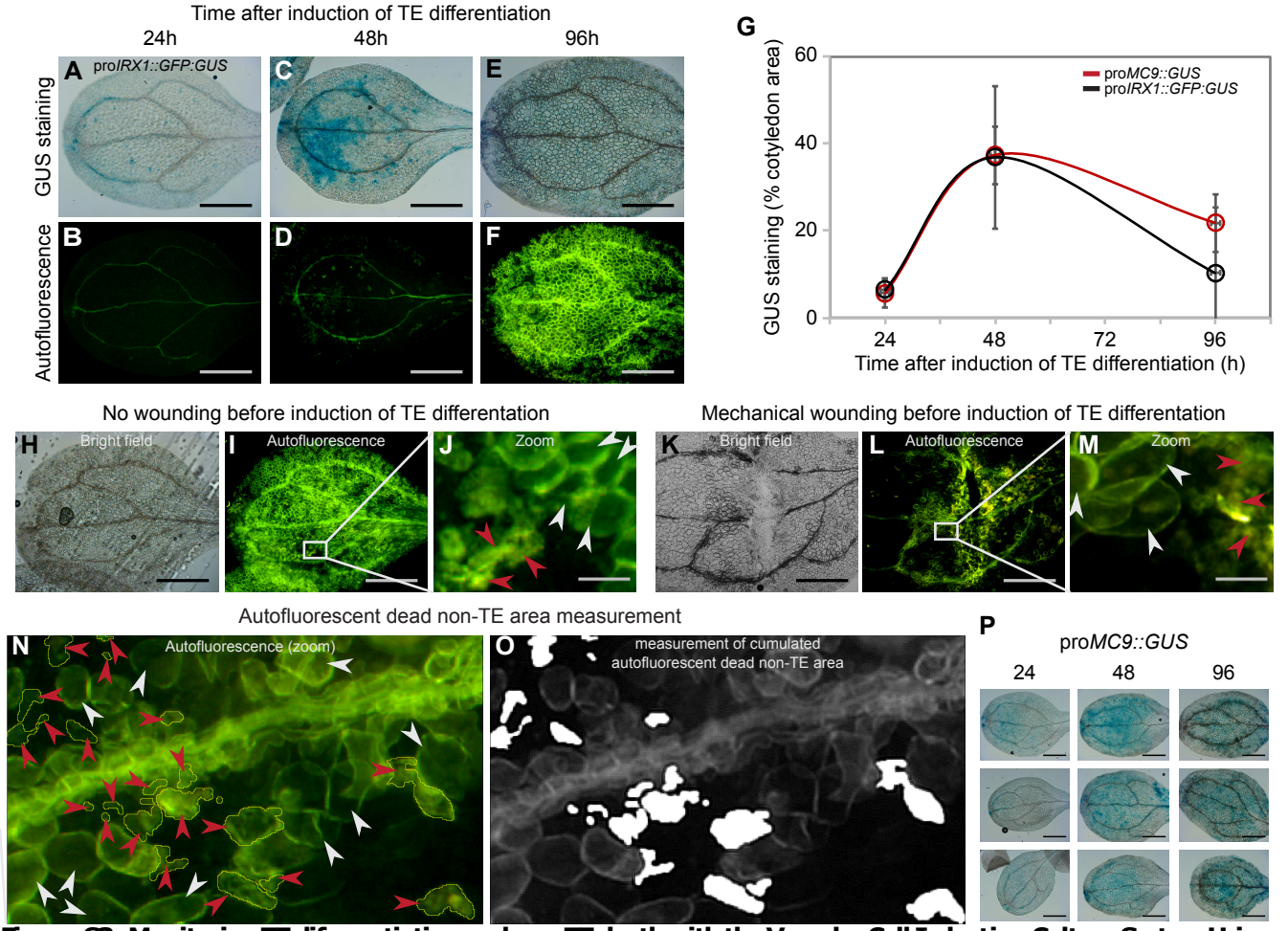

Figure S3: Monitoring TE dif erentiation and non-TE death with the Vascular Cell Induction Culture System Using Arabidopsis Leaves (VISUAL).

(A-F) Micrographs of Arabidopsis pro*IRX1::GFP:GUS* (11) cotyledons induced for TE dif erentiation using the VISUAL method (28). (A, C, and E) display GUS staining (blue) at dif erent time points after induction of dif erention. The GUS staining reports activity of the *IRX1* promoter which is specif c to the tracheary element (TE) cell type in this experimental system. The disapearance of GUS staining at the last time point is due to the developmental cell death and autolysis of the TE cell type. (B, D, and E) show autof uorescence originating mainly from lignin in the cell walls of the TE cell type, which increases over time as more TEs f nish their dif erentiation. Scale bars = 1 mm.

(G) Quantif cation of GUS signal over the course of TE dif erentiation in the cotyledons of the pro*MC9::GUS* and pro*IRX1::GFP:GUS* reporter lines. The GUS signal increases between 24h and 48h, as expected from the fact that TE cells start dif erentiating (ref. 35), while the GUS staining strongly decreases at 96h as expected from the fact that TEs undergo developmental cell death. Error bars represent standard deviation (n = 3 biological replicates).

(H-M) Micrographs of Col-0 wild-type cotyledons 96h after induction TE dif erentiation with the VISUAL methods without (H-J) or after (K-M) mechanical wounding. Ectopic non-TE cell death that occurs as a consequence of wounding (M) or as a consequence of TE dif erentiation (J) is revealed by shrunken, autof uorescent protoplasts (red arrowheads) which are absent from fully autolyzed, hollowed TE cells (white arrowheads) whose cell walls are autof uorescing. Scale bars = 1 mm in the full cotyledons micrographs and 100 µm in the corresponding zoomed images.

(N,O) Illustration of the quantif cation process of dead non-TE areas of induced cotyledons based on autof uorescence micrographs. (N) The cells displaying features of dead non-TEs (red arrows) such as shrunken autof uorescent shrunken protoplast clearly dif erent from empty TEs that only show cell wall autof uorescence (white arrows) were selected using the "selection brush tool" in ImageJ and there cumulated area over the entire cotyledon was measured as illustrated in (O).

(P) Micrographs of GUS histochemical staining for pro*MC9::GUS* quantif ed in (g). Remainder GUS signal at 96h is localized in cells with visible cell wall thickenings which indicate that they are tracheary elements. Bars = 1mm

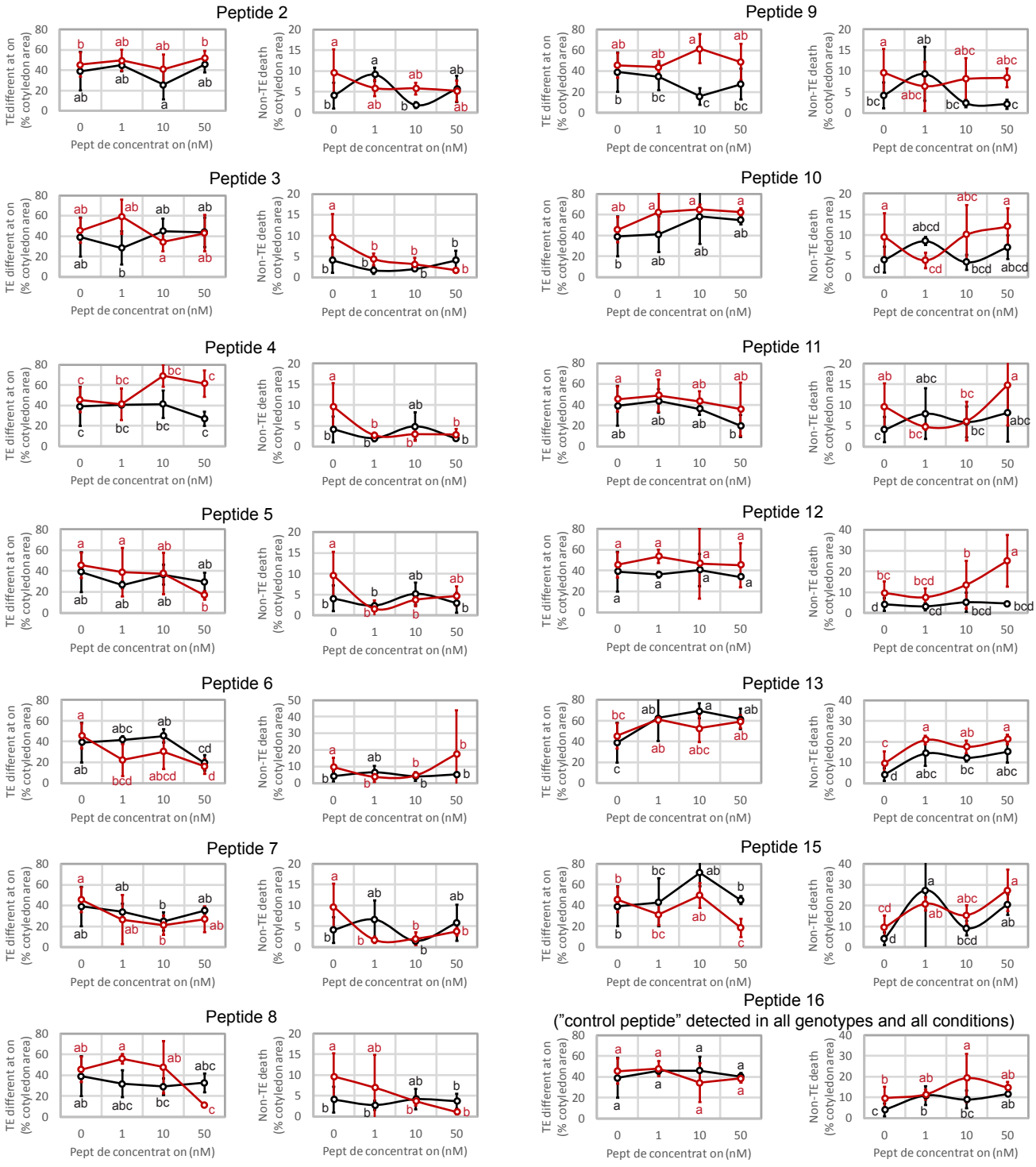

Figure S4: Ef ect of candidate peptides from crude extracts on TE dif erentiation and non-TE death

TE dif erentiation (left) and non-TE death (right) 96h after induction with the VISUAL method of Col-0 wild-type and *mc9-2* METACASPASE9 knock-out mutant treated with increasing concentrations of indicated peptide (or only phosphate buf er as a conctrol). Error bars represent standard deviation (n = 3 biological replicates). Data points that do not share any letter are signif cantly dif erent according to post-ANOVA Fischer test ($p < 0.05$).

A

```
1   MGRLVSGATL LALLCFHVFV VNVVARDVSS GRDEDEKTLV GGGKGGGFGG
51  GFGGGAGGGV GGGAGGGFGG GAGGGFGGGG GGGGGGGGGG GGGFGGGGGF
101 GGGHGGGVGG GVGGGHGGGV GGGFGKGGGI GGGIGKGGGV GGGIGKGGGI
151 GGGIGKGGGV GGGIGKGGGI GGGIGKGGGI GGGIGKGGGI GGGIGKGGGI
201 GGGIGKGGGV GGGFGKGGGV GGGIGKGGGV GGGFGKGGGV GGGIGKGGGI
251 GGGIGKGGGI GGGIGKGGGI GGGIGKGGGI GGGIGKGGGI GGGIGKGGGI
301 GGGIGKGGGI GGGIGKGGGI GGGGGFGKGG GIGGGIGKGG GIGGGGGFGK
351 GGGIGGGIGK GGGIGGGFGK GGGIGGGIGG GGGFGGGGGF GKGGGIGGGI
401 GKGGGFGGGG GFGKGGGIGG GGGFGKGGGF GGGGFGGGGG GGGGGGGGIG
451 HH
```

Sequence repeats

GGGIGGGIGK * 16

GGGVGGGIGK * 4

GGGIGGGFGK * 3

Predicted signal peptide

Predicted transmembrane domain

B

```
1   MTRGSQRERD RERALARTGG KGKNKDDGLT PEQRRERDAK ALQEKTAKKA
51  AQAAAAASSG GGGGKGNNK
```

Predicted:
Nucleus or mitochondrial

C

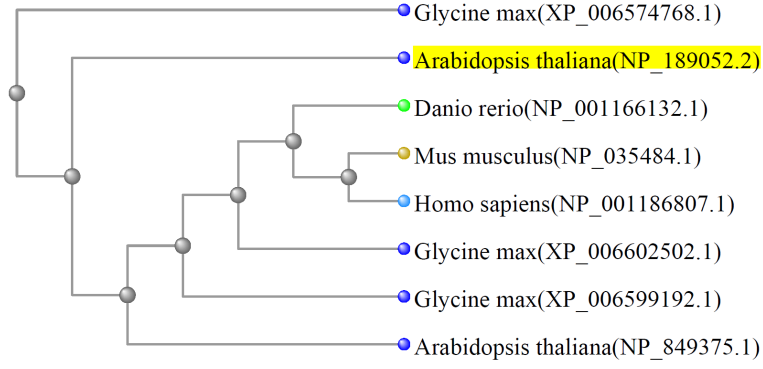

Figure S5: Sequences of the precursor proteins from which the peptides Kratos and Bia are generated.
(A) Sequence of the protein from which the Kratos peptide is generated. Predicted motifs based on protein sequence are highlighted with colors and described below the sequence, while the Kratos peptide is underlined.
(B) Sequence of the protein from which the Bia peptide is generated. Predicted localization based on protein sequence is indicated below the sequence, while the Bia peptide is underlined.
(C) Phylogenetic tree of SERF family proteins, using the precursor protein from Bia/Peptide 14 as query (highlighted) for protein BLAST in NCBI, against the "Model Organisms" database. Multiple Protein alignment and phylogenetic tree were generated using COBALT (Papadopoulos JS and Agarwala R, 2007. Bioinformatics 23:1073-79) using the "Fast Minimum Evolution" method.

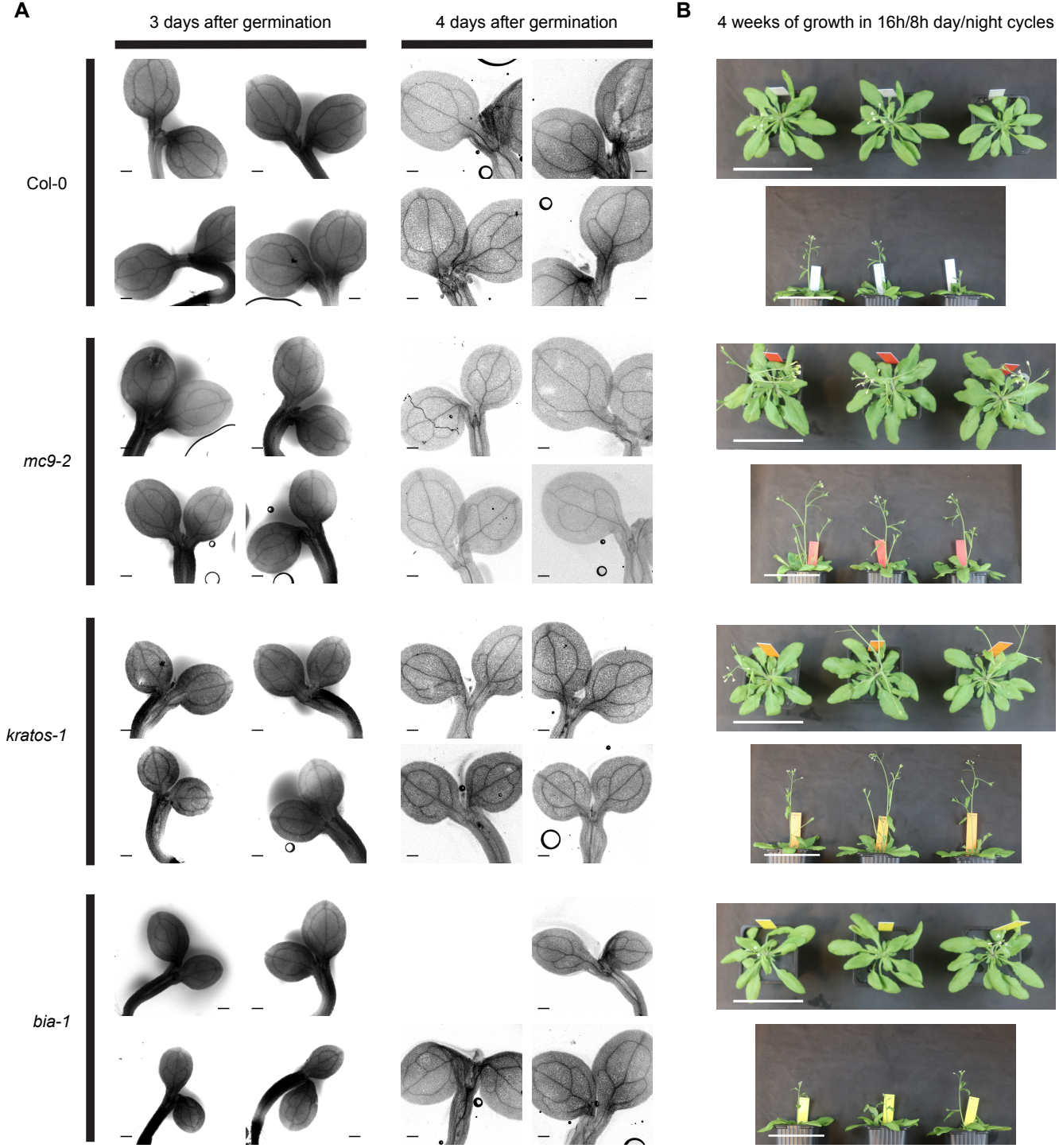

Figure S6: Normal vascular development in the cotyledons of the *mc9-2*, *bia-1* and *kratos-1* mutants.
(A) Micrographs of the Col-0, *mc9-2*, *bia-1* and *kratos-1* seedlings stained with Evans blue (stains mostly dead vascular tracheray elements, used here to highlight vasculature), imaged 3 and 4 days after germination. Bars = 200 µm.
(B) Images showing 4-weeks-old plants of the Col-0, *mc9-2*, *bia-1* and *kratos-1* genotypes grown in standard greenhouse conditions (16h/8h day/night cycle, and 18°C < temperature < 23°C). Bars = 10cm
The pattern of vasculature (clearly visible from the Evans blue staining of dead vascular TEs) did not appear to clearly dif er between the genotypes and the apparently normal growth of all mutants suggest normal vascular development, at least in optimal growth conditions.

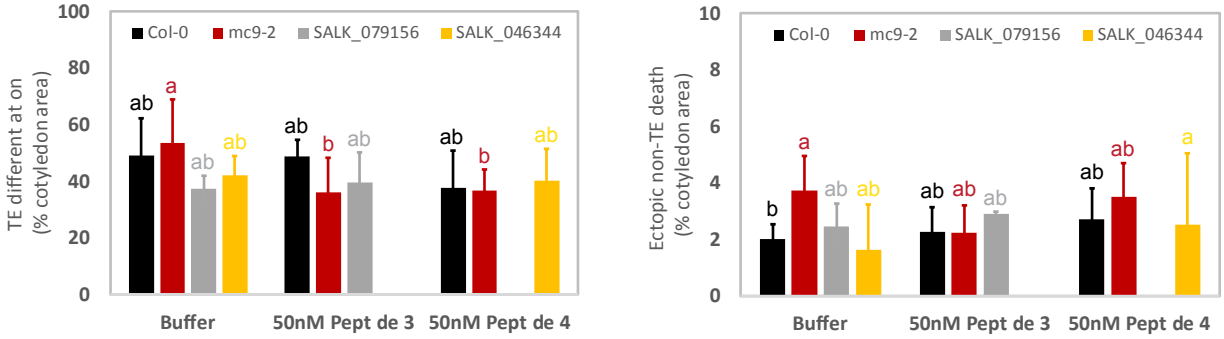

Figure S7: Peptides 3 and 4 do not af ect non-TE death.

TE dif erentiation (left) and non-TE death (right) 96h after induction with the VISUAL method of Col-0, *mc9-2*, peptide 3 knock-out mutant (SALK_079156) and peptide 4 knock-out mutant (SALK_046344) treated or not with 50 nM Peptide. Error bars represent standard deviation (n = 3-9 replicate experiments). Data points that do not share any letter are signif cantly dif erent according to post-ANOVA Fischer test ($p < 0.05$).

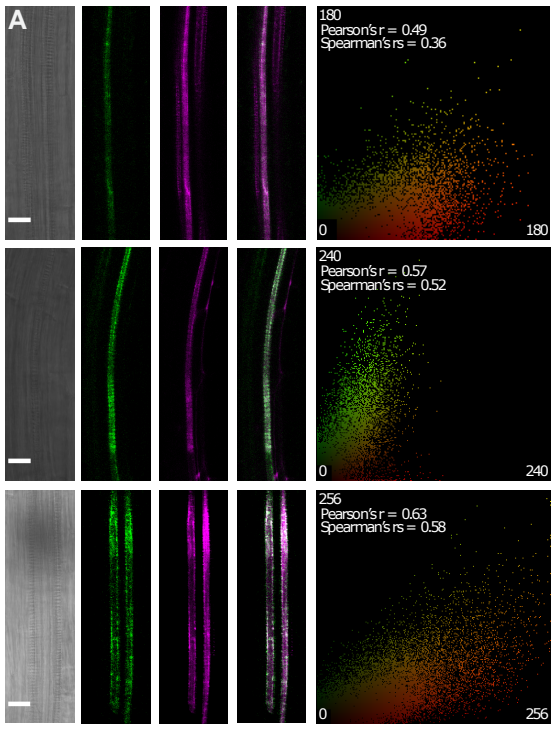

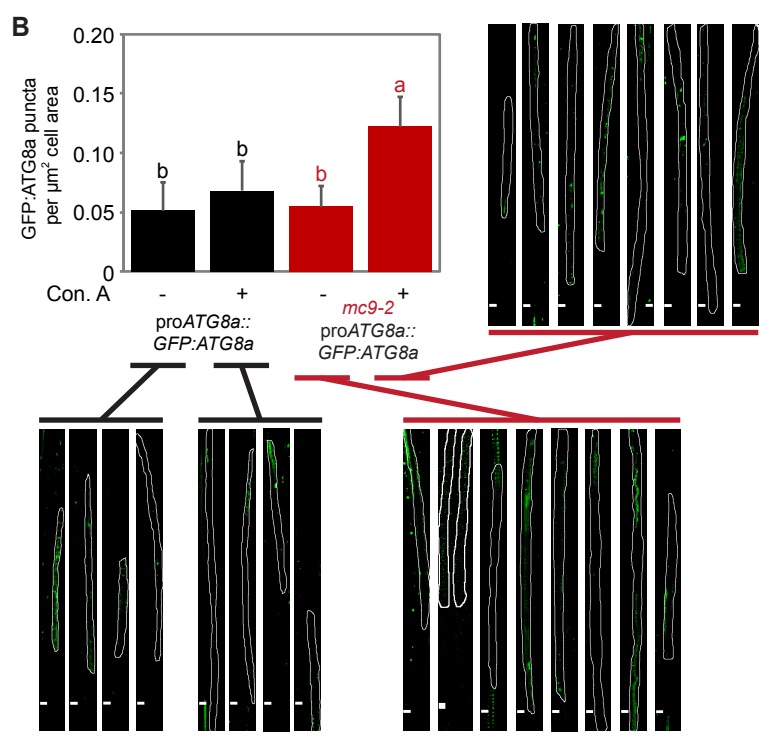

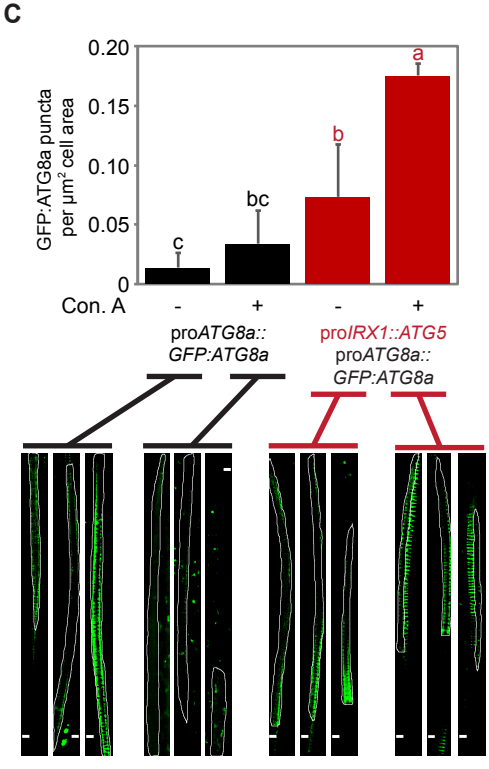

Figure S8: METACASPASE9 and autophagy are linked in TEs.
(A) Confocal Laser Scanning Microscopy imaging of tracheary elements in the roots of three Arabidopsis seedlings harboring proMC9::MC9:mCherry (Bollhöner *et al.*, 2013) and proATG8a::GFP:ATG8a (Furuta *et al.*, 2014) translational fusions, after 2 h treatment with 10µM Concanamycin A to inhibit autophagosomal degradation. Correlations between GFP and mCherry signal on each pixel was calculated using the Pearson-Spearman Correlation (PCS) colocalization plugin in Image J.
(B-C) Images and quantif cation of GFP:ATG8a puncta (indicating autophagosomes) in these confocal laser scanning micrographs of the f rst dif erentiating xylem cells in a cell f le (from the root tip) displaying detectable levels of GFP:ATG8a (driven by the pro*ATG8a* endogenous promoter active in TEs, as in (A)). Both pro*ATG8a::GFP:ATG8a* marker lines in wild-type background, or introgressed in *mc9-2* (B) or pro*IRX1::ATG5* TE autophagy overexpressor (C) were observed after propidium iodide staining (allowing to recognize TEs based on their cell wall patters, Escamez *et al.*, 2016), without or after 3h treatment with 10µM Concanamycin A (Con. A), which stops autophagic f uxes and allows accumulation of autophagosomes (*Escamez et al.*, 2016). Values that do not share any letter are signif cantly dif erent ($p < 0.05$) according to a post-ANOVA Fisher test (n = 3-8 biological replicates). The displayed micrographs represent the GFP-ATG8a detection channel after thresholding of the f uorescence signal to help distinguishing autophagosomes from the dif use GFP signal typical for GFP-ATG8 markers. The white shape outlines the part of the recorded TE that is in the analyzed focal plane (as the cells are neither f at nor perfectly straight compared with the lens, the entire cell surface is rarely entirely visible in a single focal plane). Bars = 5µm.

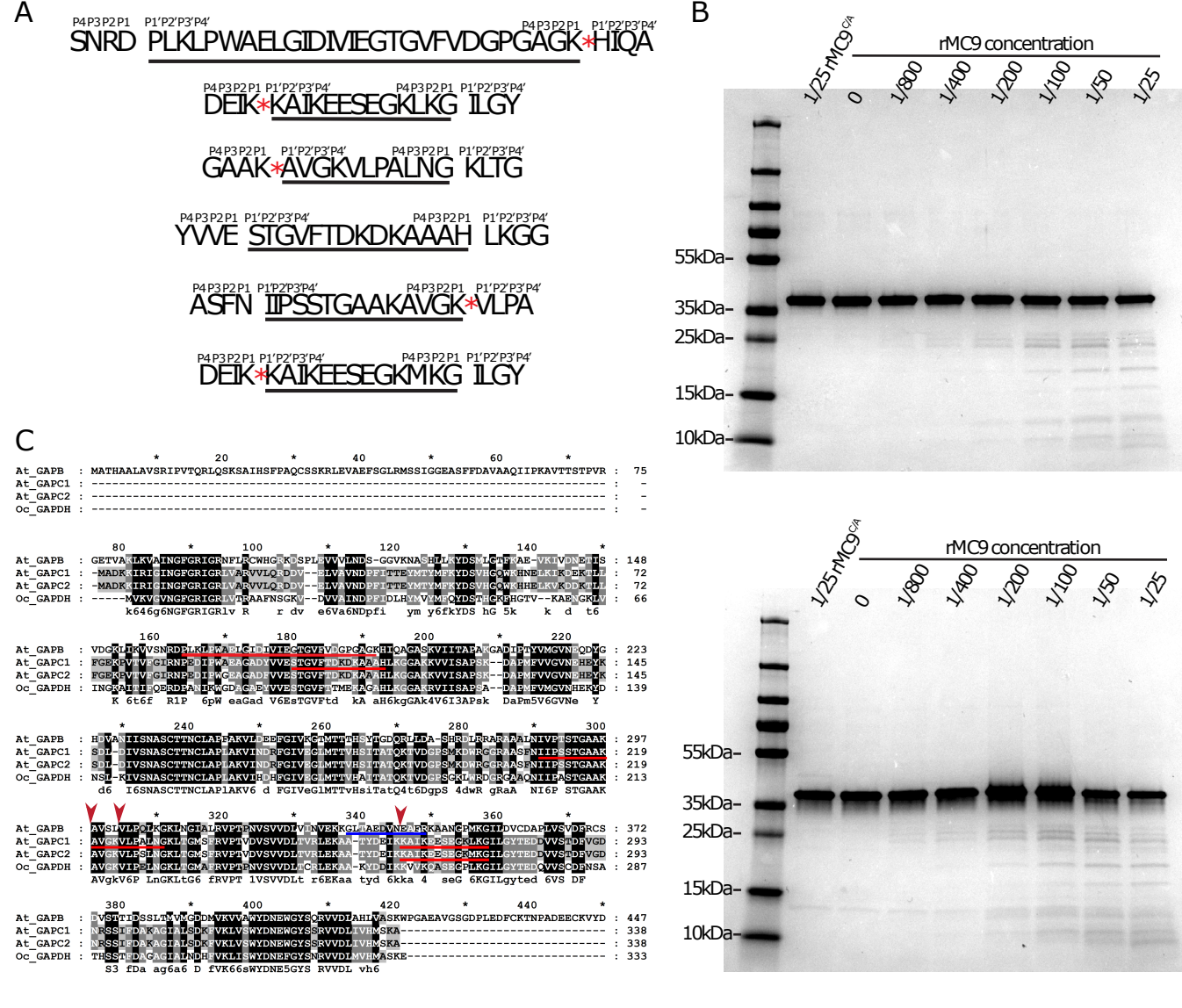

Figure S9: GAPDH peptides are detected in extracellular peptidomics of dif erentiating cells, possible from cleavage of GAPDH by MC9.

(A) Sequences of the six peptides originating from three GAPDH subunits (underlined) with the four amino acids from the corresponding precursor proteins around both the N-terminal and C-terminal cleavage sites (indicated by spaces). Red asterisks indicate cleavage sites compatible with METACASPASE9 favoured target sequences (Henry *et al.*, 2015).
(B) Commercially available GAPDH proteins (top GAPDH solution from rabbit muscle, product name G5262 from Sigma; bottom lyophilized GAPDH from rabbit muscle, product name G2267 from Sigma) were incubated with increasing amounts of recombinant MC9 (rMC9) or with an inactive version MC9 $^{C/A}$, as control, for 30 minutes at 30 C.
(C) Multiple sequence alignment of the *Arabidopsis thaliana* GAPDH proteins (At_GAPB, At_GAPC1 and At_GAPC2) identif ed in this study with Oryctolagus cuniculus (rabbit) GAPDH (Oc_GAPDH; UniProtKB - P46406). Peptides identif ed in this study are underlined in red. A neo-N-terminal peptide previoustlt identif ed as potential substrate of rMC9 in (Tsiatsiani *et al.*, 2013) is underlined in blue. Red arrowheads indicate potential MC9 cleavage sites based on known MC9 recognition sites and on the observation of peptides in the peptidomics analysis in this study derived from cleavage at the indicated positions (A).

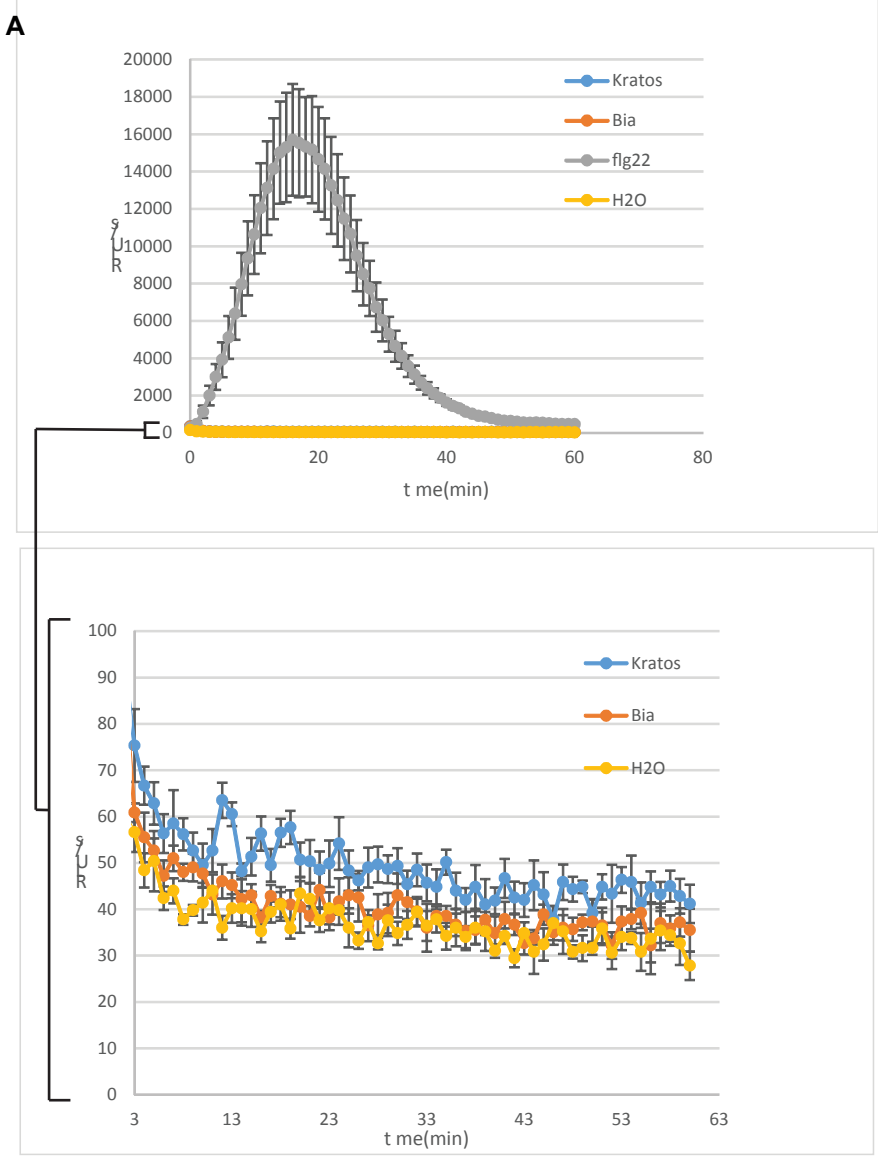

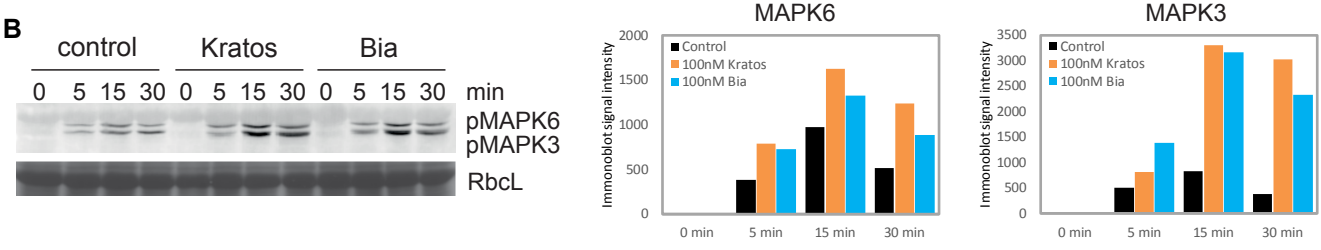

Figure S10: Kratos and Bia do not trigger oxidative burst.
(A) Reactive Oxygen Species (ROS) burst measurements in response to treatments with the peptides Kratos, Bia and Flg22 (all 100 nM). Flg22 was used as a positive control, while water was used as a negative control.
(B) Immunoblot (left) and the corresponding quantif cation (right) of mitogen-activated protein kinase (MAPK) activation in response to peptide inf ltration (100 nM) to Col-0 rosette leaves. The control is constituted by inf ltration with buf er alone (10 mM sodium phosphate, pH 7). Immunoblot of the large subunit of Rubisco (RbcL) was used as a loading control.

Table S1. List of the unique peptides selected for analyses during vascular differentiation.

Peptide ID (in this study)	Peptide sequence	Gene ID	Gene annotation	Reason(s) for selecting this candidate	Vascular expression*
Kratos/Peptide 1	**GGIGKGGGIGGGIGKGGGIG**	AT3G23450	unknown function	Significant difference in peptide analysis (Dataset S1). Abundant in induced wild-type but nearly absent in *MC9*-RNAi. The full protein seems to be a repeat of this peptide.	Yes
Peptide 2	**DSTQIHTHM**	AT5G17920	Methione Synthesis	Pepetide abundant in induced *MC9*- RNAi but not found in wild-type.	Yes
Peptide 3	**AVYQRSGGAPGGAGGE**	AT5G28540	BIP1, Luminal-binding protein 1, HSP70	Pepetide abundant in induced *MC9*- RNAi but not found in wild-type.	Yes
Peptide 4	**FYVVTDPRDDNPVNPRPGT**	AT1G04680	Pectate Lyase, PLA1, lateral root emergence	Pepetide abundant in induced *MC9* -RNAi but not found in wild-type. The corresponding gene is involved in lateral root emergence, a process which also involves MC9.	Yes
Peptide 5	**LVIIPAGVPRKPG**	AT1G53240	MITOCHONDRIAL MALATE DEHYDROGENASE 1 (mMDH1)	Pepetide abundant in induced *MC9* -RNAi but not found in wild-type.	Yes
Peptide 6	**YVSIPIEGPYKPPH**	AT4G13940	HOMOLOGY-DEPENDENT GENE SILENCING 1 (HOG1)	Pepetide indentified in all conditions and genotypes except in induced *MC9*- RNAi.	Yes
Peptide 7	**TTDFPKNPPH**	AT2G38080	IRREGULAR XYLEM 12 (IRX12), laccase activity, Laccase-4	Peptide abundant only under the induced condition. The full protein is known to localize to the apoplast. The peptide contains 3 prolines, which is common for signaling peptides.	Yes
Peptide 8	**APPPMSDAHTINGKPGPL**	AT5G03260	LACCASE 11 (LAC11)	Peptide abundant only under the induced condition. The full protein is known to localize to the apoplast. The peptide contains 4 prolines, which is common for signaling peptides.	Yes
Peptide 9	**VGDVTATIVGGLNSQNPGIQK**	AT3G10080	RmlC-like cupins superfamily protein	Peptide abundant only under the controlled condition, mostly in the *MC9* -RNAi genotype.	Yes
Peptide 10	**IVNSFKTIDG**	AT1G04680	Pectin lyase-like superfamily protein	Peptide abundant only in the *MC9* -RNAi genotype.	Yes
Peptide 11	**SSAGQVDGKQ**	AT1G76160	SKU5 SIMILAR 5 (sks5)	Significant difference in peptide analysis (Dataset S1). Pepetide indentified in all conditions and genotypes except in induced *MC9* -RNAi.	Yes
Peptide 12	**RYSNSAGGVSGPIPGGPT**	AT1G76160	SKU5 SIMILAR 5 (sks5)	Significant difference in peptide analysis (Dataset S1). Abundant in induced wild-type but nearly absent in *MC9*-RNAi.	Yes
Peptide 13	**FETEPIGKGKNGKD**	AT2G05710	ACONITASE 3 (ACO3)	Significant difference in peptide analysis (Dataset S1). Abundant in induced wild-type but nearly absent in *MC9*-RNAi.	Yes
Bia/Peptide 14	**EKTAKKAAQAAAAASSGGGGGKGNNK**	AT3G24100	Uncharacterised protein family SERF	Pepetide abundant in induced *MC9* -RNAi but not found in wild-type.	**no data available**
Peptide 15	**AKADVEPKAAEAETKPSQV**	AT3G56240	COPPER CHAPERONE (CCH)	Peptide abundant only in the induced condition. Potential MC9 substrate	Yes
Peptide 16	**NAIGGRKGRIYVVTDPANDDPVNPRPGT**	AT3G27400	Pectin lyase-like superfamily protein	Peptide abundant in all conditions for all genotypes, therefore representing a potential control peptide.	Yes

* We considered as ”vascular expression” the detection of transcripts in tracheary elements (TEs) or in any cell neighboring TEs (i.e. pro-cambium, xylem-pole pericycle) in the Arabidopsis eFP Browser (Winter et al. 2007. *Plos One* **2**(8): e718) ”Root” dataset, consisting of transcriptomics data from different root cell types (Brady et al. 2007. *Science* 318(5851): 801-806; Cartwright et al. *2009*. *Bioinformatics* 25(19): 2581-2587).